Frequency domain response analysis

A THESIS

submitted by

VISHARAD JAYDAS BORSUTKAR

in partial fulfillment of the requirements
for the award of the degree of

MASTER OF TECHNOLOGY

DEPARTMENT OF OCEAN ENGINEERING

INDIAN INSTITUTE OF TECHNOLOGY, MADRAS

May 9, 2023

THESIS CERTIFICATE

This is to certify that the thesis titled **Frequency domain response analysis**, submitted by **Visharad Jaydas Borsutkar**, to the **Indian Institute of Technology, Madras**, for the award of the degree of **Dual Degree**, is a bona fide record of the research work done by him under my supervision. The contents of this thesis, in whole or in parts, have not been submitted to any other Institute or University for the award of any degree or diploma.

Name of Guide:

Dr. Abhilash Somayajula

Department of Ocean Engineering

IIT Madras

Name of student:

Visharad Jaydas Borsutkar

Department of Ocean Engineering

IIT Madras

Signature:

Signature:

Place: Chennai, Tamilnadu 600036

Date: 8 May 2023

ACKNOWLEDGEMENTS

Words cannot express my gratitude to my supervisor, **Dr. Abhilash Somayajula**, without whom this would have been impossible. I am deeply indebted to him for his constant guidance and motivation which helped me grow professionally and personally. His mentorship is not limited to research, and I am also thankful to him for his encouragement and advise regarding graduate program applications.

I would also like to acknowledge **Dr. Sriram V**, **Dr. Deepak Kumar** and **Dr. Abhilash Somayajula**, members of my dual degree project review commitee, for their input and suggestions that helped my work.

I am grateful to **MAV lab** of IIT Madras for allowing me participate in the research work and research seminars that immensly helped for my DDP work.

Last but not the least, I would like to express gratitude to my family for their unconditional support throughout my entire study at IIT Madras.

ABSTRACT

Anticipating the ship's movements is a critical aspect that needs to be considered both in the initial design phase and later during the ship's service life. It is essential to comprehend the motion characteristics of the vessel in all six degrees of freedom to ensure safe operation in challenging marine environments.With the increasing number of large ships, there is a need to anticipate their optimal performance concerning travel time, fuel efficiency, as well as ensuring the security of cargo and personnel along specified shipping routes. This can be accomplished by employing user-friendly and effective numerical tools that can predict the hydrodynamic loads acting on floating vessels when moving at a constant forward speed and calculate their motion responses in diverse wave conditions as per the requirements. The current dissertation outlines the integration of a three-dimensional potential theory-based approach, developed in Python, which takes into account the effects of forward speed. This paper elucidates the theoretical formulation, numerical implementation, as well as the comparisons with the outcomes of different programs. Additionally, the thesis discusses the near-field approach employed to calculate the mean drift force.

As a part of this dual degree project, a method to compute the wave forces and motions with the forward speed effect has been added into the web-based analysis tool **HydRA** developed by the students of MAV lab students of IIT Madras. KCS and KVLCC2 ship hull forms are analyzed and validated against the MDLHydro software developed by Dr. Amitava Guha. The comparison results are found to be in excellent agreement.

Keywords : Potential theory, laplace equation, boundary element method (BEM), Hydrodynamic, Wave structure interaction, multibody interaction, forward speed, mean drift force.

TABLE OF CONTENTS

LIST OF TABLES

LIST OF FIGURES

ABBREVIATIONS

DftFrc   Drift force

FkFrc   Froude Krylov force

ScFrc   Scattering force

GCS   Global coordinate system

BCS   Body coordinate system

RAO   Response amplitude operator

NOTATIONS

$\boldsymbol{\phi_T}$ Total potential

ϕ_I Incident potential

ϕ_D Scattering potential

ϕ_j radiation potential in j_{th} mode of motion

$\vec{x}_s$ location of Source

ω_I Incident wave frequency

ω_e Encountering wave frequency

U Forward speed

g acceleration due to gravity

σ source strength

n_k unit vector in k_{th} direction

β wave incident angle

dS Panel surface area

ϵ perturbation parameter

$\vec{T}^{(2)}$ second order term

η_j wave motion RAO for j^{th} mode of motion

A_{ij} Added mass in j^{th} mode of motion due to oscillation along k^{th} direction

B_{ij} Radiation damping in j^{th} mode of motion due to oscillation along k^{th} direction

F_I^k Froude krylov force for k^{th} mode of motion

S_I^k Scattering force for k^{th} mode of motion

CHAPTER 1

INTRODUCTION

1.1   Objective

This Dual Degree project aims to achieve two primary goals. The first objective is to calculate the motion characteristics and forces on a floating structure traveling at a low to moderate forward speed in regular waves for the frequency domain hydrodynamic analysis tool **HydRA**. This computation is done by utilizing a 3D panel-based potential theory method that involves using an infinite-depth green function. The second objective is to compute the second-order forces i.e. mean drift force. The implementation is done by keeping in mind that this method can be used for single body case as well as for multibody case. Also, then the program's output is validated against the MDLHydroD software.

The thesis is structured in the following manner. The first chapter includes an introduction, the objectives of the project, the background and motivation, and a literature review. The second chapter provides an explanation of the mathematical problem setup and derivation. Chapter 3 illustrates the solution to the numerical mathematical problem. Chapter 4, elaborates on the calculation of wave forces and motions. Likewise, Chapter 5 describes the computation of drift force. In the last chapter, the project outcomes are compared with other software tools such as MDLHydroD and WAMIT6.

1.2   Background and Motivation

A floating object is exposed to multiple forces, such as wind, currents, waves, and other environmental loads. The issue of sea-keeping involves the computation

of hydrodynamic parameters and forces acting on a floating structure when it is in waves. To solve the problem of wave-body interaction, hydrodynamic forces are calculated using numerical methods and potential theory. These calculations can then be used to compute the RAOs (response amplitude operator) of different types of vessels.

Hydrodynamic analysis software can help naval architects optimize and enhance the design of vessels in regular waves. It can provide insights into vessel's performance in various wave conditions, allowing designers to make informed decisions about the shape and size of the vessel. Moreover, it saves costs by reducing the need for expensive physical testing. Software for hydrodynamic analysis can allow designers to iterate designs faster, as they can quickly simulate and evaluate the performance of different design configurations. This can help reduce the time-to-market for new vessels and increase productivity.

The primary goal of this project is to develop a flask-based web application named 'HydRA' capable of computing hydrodynamic properties such as Froude Krylov force, scattering force, RAO, radiation damping, and Added Mass for a vessel in zero and non-zero speed scenarios. Also, the implementation of drift forces captures the effect of second-order forces in the deep sea. The main idea behind building an in-house web application is to have a solid foundation for a hydrodynamic analysis tool that can be further improved and extended toward more complex problems. The work outlined in the thesis closely adheres to the study presented in Guha and Falzarano (2015*b*) and Guha (2012).

1.3   Literature review

During the initial phases of ship design, it is vital to have knowledge about the vessel's stability to ensure efficient and safe operation at sea. Evaluating hydrodynamic forces and motion features of the ship in regular waves is an essential factor for designing a stable and secure vessel. As computational power has become more accessible, computational fluid dynamics (CFD) has become more

popular in solving problems related to the interaction between fluids and structures. Despite advancements in CFD, it is a still time consuming process to predict responses. Therefore, CFD may not be a practical option during the preliminary design stage. Since, CFD is not feasible during the early stages of design due to its time-consuming nature, potential theory based methods are still widely used for designing floating structures like oil production platforms, offshore wind turbines, wave energy converters, etc. The potential theory method has been advanced by the strip theory approach, which involves dividing a ship into multiple 2D strips along its length. By combining solutions to various two-dimensional problems, the three-dimensional hydrodynamics problem can be determined. Many researchers have contributed to the development of this approach which includes Newman (1979), Ogilvie and Tuck (1969), Beck and Troesch (1990), Journée (2001), Salvesen *et al.* (1970). Beacause, the strip theory method assumes the bodies are slender, it was not suitable for analyzing ship structures and offshore stuctures which have a non-slender shape. Therefore, a 3D panel based potential theory was developed. In this method, the floating vessel is descritized or is a mesh of quadrilateral or triangular panels with different source strengths.

Tuck and Faltinsen 1970 Salvesen *et al.* (1970) provides a detailed review of the theoretical and mathematical models used to predict the motion of ships in waves and the resulting sea loads acting on the hull, which is based on the pressure distribution around the hull and the wave-induced accelerations. The paper covers the effects of ship design parameters, wave steepness and frequency, and wave-induced motions on ship motions. It presents a mathematical model for calculating the sea loads acting on the hull. The paper then discusses the effect of ship design parameters, such as beam and draft, on ship motions and the influence of wave steepness and frequency.

The calculation of the Green function efficiently for frequency and time domain analyses has been a long-standing research area. Newman (1979) provides a comprehensive list of methods to compute both frequency domain and time domain Green functions efficiently. Similar work on the zero speed frequency domain Green function has also been reported by Telste and Noblesse (1986). It describes

the theoretical background of the green function and the numerical method used to evaluate it.

The book Liapis (1986) is considered very important book for studying dynamics of ships and floating structures. The book focuses on the time-domain analysis of ship motions and provides an in-depth discussion of various methods for solving the differential equations of motion for ships in time-domain, including numerical and analytical methods. This book also explains about the equations shown in the section 3.2.

Guha and Falzarano (2013) and Guha and Falzarano (2015b) discuss developing and validating a frequency domain program that uses numerical methods for predicting the motion and hydrodynamic forces acting on floating bodies, specifically ships.

When a floating body is subjected to ocean waves, it experiences not only first-order forces (linear wave forces) but also second-order forces, which are nonlinear in nature. The second order forces are better known by their physical effects on a floating body as the added resistance or the mean drift forces Second order forces become important when wave induced motions are large. Primarily, mean drift forces are computed using two menthods: (a) far field method and (b) near field method.

Far field method was introduced by Maruo (1957) which is based on diffracted and radiated wave energy and momentum flux at infinity. The paper analyzes the experimental data of model tests and the calculations based on hydrodynamic theory to estimate the additional resistance or mean drift force on the ship due to wave-induced effects. The study indicates that the additional resistance is proportional to the square of the wave amplitude and frequency, which is consistent with the second-order wave theory.

Near field method was introduced by Boese (1970) which is based on direct integration of pressure on submerged surface in short uses potential theory. This paper, describes a simple method for calculating the increase in resistance of a ship

in waves. The method involves calculating the wave drag of the ship at zero speed and then using a correction factor to account for the effect of waves on the ship's resistance.

Faltinsen (1980), Pinkster (1980) talks about the derivation of the equations for mean drift forces and also about the second order wave theory. Faltinsen (1980) presents a method to predict the added resistance or drift force and propulsion of a ship in a seaway. The method is based on the potential theory and takes into account the effects of wave-induced motions on the ship's performance. The paper provides a detailed description of the theoretical background and numerical implementation of the method using the perturbation theory. Faltinsen also presents experimental results that validate the accuracy of the method. This paper is a significant contribution to the field of ship hydrodynamics, providing a reliable and practical approach to predicting ship performance in a seaway. Pinkster (1980) concludes that second-order wave forces can have a significant effect on the motions and loads of floating structures and should be considered in the design of offshore structure.

This project documents the development of added feature i.e. to be able to perform analysis with the effect of forward speed for simple single body case as well as for complex multi-body case for the "HydRA" tool being developed in the research guild group at IIT Madras. In addition to that theory about drift force and its solution is also discussed.

CHAPTER 2

MATHEMATICAL MODEL

In this thesis, a ship moving with a steady speed of U in deep water with regular waves of wave amplitude A and incident frequency w_I traveling at an angle β relative to the surge direction of the ship is considered. To address the seakeeping problem, potential flow techniques are commonly employed. With the advancements in computing power, it is now possible to use the three-dimensional panel based potential theory method to compute the wave load.

2.1 Co-ordinate System

In order to set up the mathematical model, two co-ordinate systems are defined; one of them is the Global co-ordinate system (GCS), whose origin is located at a calm water level. The other one is the Body seakeeping co-ordinate system (BCS), whose origin is located at the mid-ship on the intersection of the water line and centerline of the ship. It is further assumed that the x-axis of the GCS points towards the east direction, whereas the x-axis of BCS points towards the sway direction of the ship. Co-ordinates of points represented in GCS are expressed as $\boldsymbol{x^e} = (x^e, y^e, z^e)$ whereas for the points in BCS it is expressed as $\boldsymbol{x^s} = (x^s, y^s, z^s)$. Global co-ordinate system, i.e., GCS, denotes the inertial frame of reference. Body geometry and body parameters, such as the location of the vertical center of gravity and radii of gyration, are defined with respect to BSC. The translating frame of reference, BCS allows the formulation of the vessel response in six degrees of freedom due to incident waves and steady current of speed U in $-x$ direction which is equivalent to forward speed with respect to GCS. By assuming a small wave amplitude, a linear boundary value problem can be established to determine the velocity potential.

2.2 Velocity potential

Assuming that the fluid flow is inviscid, incompressible, and irrotational the total velocity potential at any point inside the fluid domain is given as :

$$\mathbf{\Phi}(\vec{x},t) = \left[-Ux+\phi_P(\vec{x})\right]+\left[\phi_I(\vec{x},\beta,\omega_I)+\phi_S(\vec{x},\beta,\omega_I)+\sum_{j=1}^{6} n_j\phi_j(\vec{x},U,\omega_e)\right]e^{iw_et}$$

(2.1)

where,

- ω_I is the incident wave frequency.

- ω_e is the encountering wave frequency.

- $\phi_P(\vec{x})$ is the potential due to the perturbation of steady translation of stream.

- $\phi_I(\vec{x},\beta,\omega_I)$ is the incident potential due to incident waves.

- $\phi_S(\vec{x},\beta,\omega_I)$ is the scattering potential due to the reflected waves from the body.

- $\phi_j(\vec{x},U,\omega_e)$ is the radiation potential generated due to the motion of body in j^{th} mode of motion.

In the above equation, the perturbation potential ϕ_P has a relatively insignificant effect on the total potential at low to moderate ship speed and so it is ignored to reduce the complexity of the problem. Hence, the final equation for velocity potential is given as :

$$\mathbf{\Phi}(\vec{x},t) = -Ux + \left[\phi_I(\vec{x},\beta,\omega_I) + \phi_S(\vec{x},\beta,\omega_I) + \sum_{j=1}^{6} n_j\phi_j(\vec{x},U,\omega_e)\right]e^{iw_et} \quad (2.2)$$

In the above equation, ω_I is the frequency of the wave experienced by the vessel when it is stationary. According, to the Doppler effect the actual frequency experienced by a body with steady speed is different from the incident frequency of the source. Hence, in this problem, ω_e is the frequency of the wave experienced by the vessel when it is moving with a certain steady speed U, which is expressed in terms of incident or normal wave frequency ω_I , forward speed U, and incident angle β

as :

$$\omega_e = \omega_I - \frac{\omega_I^2}{g} U \cos \beta \tag{2.3}$$

2.3 Governing equation

The governing equations of the fluid flow are the continuity equation (conservation of mass) and the Navier-stokes equation (conservation of momentum). Under the assumption of inviscid and irrotational flow, the Navier-stokers equations reduce to Laplace equation given as :

$$\nabla^2 \Phi(\vec{x}, t) = 0 \tag{2.4}$$

2.4 Boundary conditions

In addition to the governing equation, the velocity potential satisfies the boundary conditions over the fluid boundaries. The total boundary surface S comprises the free surface S_F, mean body surface S_B, bottom surface S_Z, and the radiation surface S_∞ bounding the horizontal infinite fluid domain. The surfaces are shown in Fig. 2.1 below.
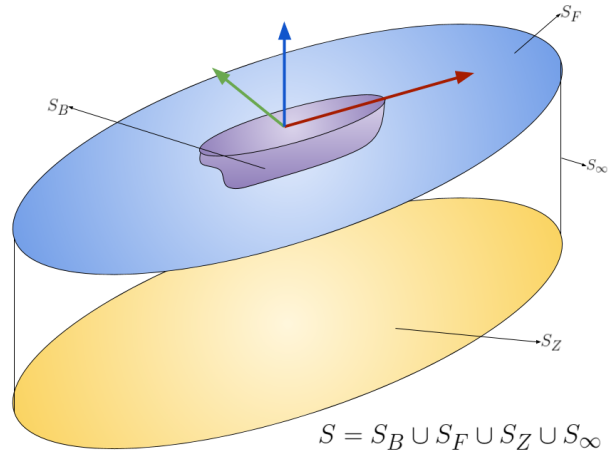
Figure 2.1: Fluid boundary surfaces

The boundary conditions to be satisfied by the potential functions are shown below:

1. Kinematic free surface boundary condition : The velocity of the fluid in the direction normal to the free surface is equal to the velocity of the free surface. If the free surface is given by $z = \eta(t, x, y)$, then the boundary condition is given by

$$\frac{\partial \eta}{\partial t} = \frac{\partial \phi}{\partial z} - \frac{\partial \phi}{\partial x}\frac{\partial \eta}{\partial x} - \frac{\partial \phi}{\partial y}\frac{\partial \eta}{\partial y} \quad \text{over } z \tag{2.5}$$

2. Dynamic free surface boundary condition : The pressure on the free surface is constant and is obtained by the application of Bernoulli's equation over the free surface.

$$\left[\left(i\omega_e - u\frac{\partial}{\partial x} \right) + g\frac{\partial}{\partial z} \right] (\phi_I, \phi_D, \phi_j) = 0 \quad \text{on } z = 0 \tag{2.6}$$

3. Radiation boundary condition : The waves generated by the oscillating body propagate outward from the body to ∞ in the fluid domain, unbounded horizontally. This boundary condition is also referred to as the Sommerfeld radiation condition.

$$\lim_{kr \to \infty} \sqrt{kr} \left(\frac{\partial}{\partial r} - jk \right) (\phi_j - \phi_I) = 0 \quad \text{for } i = 1, 2, \cdots 6 \tag{2.7}$$

4. Bottom boundary condition : The normal velocity of the fluid at the bottom boundary is equal to the normal velocity of the boundary. For an impenetrable seabed in deep water, the normal velocity is zero, and the boundary condition is given by

$$\frac{\partial \phi}{\partial z} = 0 \quad \text{over the bottom } z = -\infty \tag{2.8}$$

5. Body surface boundary condition: The velocity of the fluid in the direction normal to the body boundary is equal to the normal velocity of the body boundary over the instantaneous underwater surface S.

$$\frac{\partial \phi_j}{\partial n} = i\omega_e n_j + U m_j \quad \text{on } S \tag{2.9}$$

$$\frac{\partial \phi_I}{\partial n} + \frac{\partial \phi_D}{\partial n} = 0 \quad \text{on } S \tag{2.10}$$

9

Here, $\vec{n} = (n_1, n_2, n_3)$ is the unit normal pointing outward from the hull surface and $(n_4, n_5, n_6) = \vec{r} \times \vec{n}$, where, r is the position vector of a point on the surface. The linear incident wave potential satisfying the above boundary conditions is given by:

$$\phi_I = \frac{igA}{\omega_I} e^{-ik_I(x\cos\beta + y\sin\beta)} e^{kz} \tag{2.11}$$

Here, ω_I represents the incident wave frequency, not the encounter frequency. This forward speed boundary value problem can be solved using potential theory using infinite depth free surface green function. In general, free surface and body boundary conditions are non-linear and hence an exact solution is not possible. However, since the governing equation is linear its solutions can be obtained by using perturbation approach.

CHAPTER 3

NUMERICAL SOLUTION

The complex potential on the submerged surface of the vessel is the key to solving the hydrodynamic problem. Once the potential is known, all the hydrodynamic coefficients required to obtain all the vessel response, i.e., added mass, damping, excitation forces and response amplitude operator (RAO) can be calculated.

The boundary value problem described in (2.5) to (2.10) will be solved by a boundary element method. The body surface will be a suitable distribution of source singularities that satisfy the governing equation and the boundary conditions. Solving a Fredholm integral of the second kind over the discretized body boundary will determine the source strengths.

3.1   Integral equation

The velocity potential at some point (x, y, z) in the fluid domain can be expressed in terms of the surface distribution of sources.

$$\phi(\vec{x}) = \frac{1}{4\pi} \int_S \sigma(\vec{x_s}) G(\vec{x} : \vec{x_s}) \, dS \tag{3.1}$$

where, $\vec{x_s}$ denotes the source point of the body surface, $(\vec{x})$ denotes the point where the potential is being calculated, and $\sigma(\vec{x_s})$ is the unknown source strength distribution on the source point. Section (3.3) explains about the Green function. The Green function satisfies the continuity condition and all the boundary conditions, including the free surface and radiation boundary condition, except for the following normal velocity boundary condition on the hull surface, which is:

$$\frac{\partial \phi}{\partial n} = v_n \quad \text{on } S \tag{3.2}$$

Here, $v_n(x, y, x)$ is the flow normal velocity on the hull surface, after applying the velocity boundary condition given in (2.2) on the velocity potential (3.1), the below equation is obtained, also known as Fredholm integral of the second kind :

$$-\frac{1}{2}\sigma(\vec{x_s}) + \frac{1}{4\pi}\int_S \sigma(\vec{x_s})\frac{\partial G(\vec{x}:\vec{x_s})}{\partial n} = v_n \quad \text{on } S \qquad (3.3)$$

Here, $\frac{\partial G}{\partial n}$ denotes the derivative of the Green function in the outward normal direction. This normal derivative of G can be evaluated using its partial derivatives in x, y and z as :

$$\frac{\partial G}{\partial n} = \frac{\partial G}{\partial x}n_x + \frac{\partial G}{\partial y}n_y + \frac{\partial G}{\partial z}n_z \qquad (3.4)$$

Now, while calculating influence on a panel because of other source panel, the panel where the potential is being calculated and the source panel becomes the same. Due to this, frequency independent part of the green function tends to go to infinity. This case is known as singularity. To compensate for that influence, $-\frac{1}{2}\sigma$ is added into the equation according to the residual theory.

3.2 Numerical discretization

To solve (3.3), the body surface is discretized into M panels of area ΔS_m where $m = (1, 2, \cdots, M)$. Every entity presented here is computed at the centroid of the panel. Hence, the source strength as well is computed over each panels centroid. Now, for i^{th} panel (3.3) can be written as:

$$-\frac{1}{2}\sigma_i(\vec{x_s}) + \frac{1}{4\pi}\int_S \sigma_i(\vec{x_s})\frac{\partial G_i(\vec{x}:\vec{x_s})}{\partial n} = v_{n_i} \quad \text{on } S \qquad (3.5)$$

Here, the subscript i in the equation represents the entities of an individual panel.

The equation (3.5) can be re-written as:

$$-\frac{1}{2}\sigma_i + \frac{1}{2}\sum_{i=1,j=1,i\neq j}^{M}\alpha_{ij}\sigma_i = v_{n_i} \quad \text{for} \quad i = 1, 2, \cdots M \qquad (3.6)$$

Where, α_{ij} is :

$$\alpha_{ij} = \frac{1}{2\pi} \int_{\Delta S_i} \frac{\partial G(x, x_s)}{\partial n} \, dS \tag{3.7}$$

In physical terms, α_{ij} denotes the velocity induced at the ith panel in the direction normal to the surface by a source distribution of unit strength distributed uniformaly over the jth panel which is the source panel here and i^{th} panel is the influenced panel where the potential is being calculated because of the presence of other source panels.

The equation (3.6) can be written in the matrix format as :

$$[\sigma] = 2[\alpha - I]^{-1}[v_n] \tag{3.8}$$

where, I represents the unit matrix. $[\alpha]$ is an $M \times M$ cross matrix where M is the total number of panels. Similarly, (3.1) can be reduced to :

$$\phi_i = \sum_{j=1}^{M} \beta_{ij}\sigma_j \tag{3.9}$$

where, $[\beta]$ is the $M \times M$ matrix given by :

$$\beta_{ij} = \frac{1}{4\pi} \int_{\Delta S_j} G(\vec{x}_i, \vec{x}_s) dS \tag{3.10}$$

Now, the equation 3.10 can be written in the matrix form as :

$$\{\phi\} = [\beta]\{\sigma\} \tag{3.11}$$

Threfore, the boundary problem can be solved for the velocity potential on the body surface if the value of the integral of the Green function G and its derivative which is $\frac{\partial G}{\partial n}$ are known.

13

3.3 Green's function

For the calculation of radiation and diffraction potential, an infinite-depth green function is used. This Green function and its numerical solution is explained in Telste and Noblesse (1986). This green function assumes source distribution over the submerged surface of the vessel. It relates the unknown source strength to the velocity potential. Here, the green function comprises two parts: one is the frequency-dependent part, and the other is the frequency-dependent part. The Independent part represents the simple potential and interaction between the body surface and the free surface. On the other hand, the frequency dependent part is to comprise the oscillating potential due to the oscillating source. The equation of the Green function is given as

$$G(\vec{x}, \vec{x_s}, \omega_e) = \frac{1}{r} + \frac{1}{\acute{r}} + \tilde{G}(\vec{x}, \vec{x_s}, \omega_e) \tag{3.12}$$

where,

$$r = ||\boldsymbol{x} - \boldsymbol{x_s}|| = \sqrt{(x - x_s)^2 + (y - y_s)^2 + (z - z_s)^2} \tag{3.13}$$

represents the Eucledian distance between the field point $P(x, y, z)$ and source point $Q(x_s, y_s, z_s)$. The frequency used here is the encounter frequency shown in (2.3).

$$r' = \sqrt{(x - \xi)^2 + (y - \eta)^2 + (z + \zeta)^2} \tag{3.14}$$

represents the Euclidean distance between the field point $P(x, y, z)$ and point $Q'(\xi, \eta, \zeta)$, which is the image of the source point in the waterplane $z = 0$ and $\tilde{G}(\vec{x}, \vec{x_s}, \omega_e)$ represents the frequency domain part of the green function.

Now, substituting (3.12) in (3.15) and (3.10), gives the following equations for

α and β matrices :

$$\alpha_{ij} = -\frac{1}{2\pi} \iint_{\Delta S_i} \frac{\partial}{\partial n}\left(\frac{1}{r}\right) dS - \frac{1}{2\pi} \iint_{\Delta S_j} \frac{\partial}{\partial n}\left(\frac{1}{r'}\right) dS \qquad (3.15)$$

$$-\frac{1}{2\pi} \iint_{\Delta S_j} \frac{\partial G(\vec{x}_i, \vec{x}_j, \omega_e)}{\partial n} dS$$

$$\beta_{ij} = -\frac{1}{4\pi} \iint_{\Delta S_j} \left(\frac{1}{r}\right) dS - \frac{1}{4\pi} \iint_{\Delta S_j} \left(\frac{1}{r'}\right) dS \qquad (3.16)$$

$$-\frac{1}{4\pi} \iint_{\Delta S_j} \tilde{G}(x_i, x_j, \omega_e) dS$$

Here, j^{th} panel is the source panel and i^{th} panel is the feild point where potential is being calculated. In the above expressions, first two terms are frequency independent and the last term is frequency dependent which can be obtained by solving for the wavy green function.

3.4   Frequency independent part of Green function

The frequency independent part of the $[\alpha]$ matrix can be computed analytically using the expressions provided by Hess and Smith (1964). Similarly, the frequency independent terms of $[\beta]$ matrix can be evaluated using the expressions given by Katz and Plotkin (2001). Normal derivatives can be expressed as sum of dot products of normal unit vectors and the partial derivatives in x, y and z directions. Hence,

$$\iint_{\Delta S_i} \frac{\partial}{\partial n}\left(\frac{1}{r}\right) dS = n_x \iint_{\Delta S_j} \frac{\partial}{\partial x}\left(\frac{1}{r}\right) dS + n_y \iint_{\Delta S_j} \frac{\partial}{\partial y}\left(\frac{1}{r}\right) dS \quad (3.17)$$

$$+ n_z \iint_{\Delta S_j} \frac{\partial}{\partial z}\left(\frac{1}{r}\right) dS$$

Above integration is performed over the source panel ΔS_j and n_x, n_y, n_z are the unit normal components of the field panels. The integral is evaluated in local coordinate system with its origin at centroid. The coordinates of the source panel's

4 vertices are $A(x_1, y_1, 0)$, $B(x_2, y_2, 0)$, $C(x_3, y_3, 0)$ and $D(x_4, y_4, 0)$, which are in BCS coordinate system. Here, only x and y co-ordinates of the panel vertices are considered. Hence, according to Hess and Smith (1964) equations for the partial derivatives required to compute the normal derivative (3.17) are given below :

$$
\begin{aligned}
\iint_{\Delta S_j} \frac{\partial}{\partial x} \left(\frac{1}{r} \right) dS = {} & \frac{y_2 - y_1}{d_{12}} \ln \left(\frac{r_1 + r_2 - d_{12}}{r_1 + r_2 + d_{12}} \right) \\
& + \frac{y_3 - y_2}{d_{23}} \ln \left(\frac{r_2 + r_3 - d_{23}}{r_2 + r_3 + d_{23}} \right) \\
& + \frac{y_4 - y_3}{d_{34}} \ln \left(\frac{r_3 + r_4 - d_{34}}{r_3 + r_4 + d_{34}} \right) \\
& + \frac{y_1 - y_4}{d_{41}} \ln \left(\frac{r_4 + r_1 - d_{41}}{r_4 + r_1 + d_{41}} \right)
\end{aligned}
\tag{3.18}
$$

$$
\begin{aligned}
\iint_{\Delta S_j} \frac{\partial}{\partial y} \left(\frac{1}{r} \right) dS = {} & \frac{x_1 - x_2}{d_{12}} \ln \left(\frac{r_1 + r_2 - d_{12}}{r_1 + r_2 + d_{12}} \right) \\
& + \frac{x_2 - x_3}{d_{23}} \ln \left(\frac{r_2 + r_3 - d_{23}}{r_2 + r_3 + d_{23}} \right) \\
& + \frac{x_3 - x_4}{d_{34}} \ln \left(\frac{r_3 + r_4 - d_{34}}{r_3 + r_4 + d_{34}} \right) \\
& + \frac{x_4 - x_1}{d_{41}} \ln \left(\frac{r_4 + r_1 - d_{41}}{r_4 + r_1 + d_{41}} \right)
\end{aligned}
\tag{3.19}
$$

$$
\begin{aligned}
\iint_{\Delta S_j} \frac{\partial}{\partial z} \left(\frac{1}{r} \right) dS = {} & \tan^{-1} \left(\frac{m_{12} e_1 - h_1}{z r_1} \right) - \tan^{-1} \left(\frac{m_{12} e_2 - h_2}{z r_2} \right) \\
& + \tan^{-1} \left(\frac{m_{23} e_2 - h_2}{z r_2} \right) - \tan^{-1} \left(\frac{m_{23} e_3 - h_3}{z r_3} \right) \\
& + \tan^{-1} \left(\frac{m_{34} e_3 - h_3}{z r_3} \right) - \tan^{-1} \left(\frac{m_{34} e_4 - h_4}{z r_4} \right) \\
& + \tan^{-1} \left(\frac{m_{41} e_4 - h_4}{z r_4} \right) - \tan^{-1} \left(\frac{m_{41} e_4 - h_1}{z r_1} \right)
\end{aligned}
\tag{3.20}
$$

Similarly, according to Katz and Plotkin (2001) the frequency dependent integrals of the $[\beta]$ matrix (3.16) are given by the following expression :

$$
\begin{aligned}
\iint_{\Delta S_j} \left(\frac{1}{r}\right) dS = & \left[\frac{(x - x_1)(y_2 - y_1) - (y - y_1)(x_2 - x_1)}{d_{12}} \ln\left(\frac{r_1 + r_2 + d_{12}}{r_1 + r_2 - d_{12}}\right) \right. \\
& + \frac{(x - x_2)(y_3 - y_2) - (y - y_2)(x_3 - x_2)}{d_{23}} \ln\left(\frac{r_2 + r_3 + d_{23}}{r_2 + r_3 - d_{23}}\right) \\
& + \frac{(x - x_3)(y_4 - y_3) - (y - y_4)(x_4 - x_3)}{d_{34}} \ln\left(\frac{r_3 + r_4 + d_{34}}{r_3 + r_4 - d_{34}}\right) \\
& \left. + \frac{(x - x_4)(y_1 - y_4) - (y - y_4)(x_1 - x_4)}{d_{41}} \ln\left(\frac{r_4 + r_1 + d_{41}}{r_4 + r_1 - d_{41}}\right) \right] \\
& - z \left[\tan^{-1}\left(\frac{m_{12}e_1 - h_1}{zr_1}\right) - \tan^{-1}\left(\frac{m_{12}e_2 - h_2}{zr_2}\right) \right. \\
& + \tan^{-1}\left(\frac{m_{23}e_2 - h_2}{zr_2}\right) - \tan^{-1}\left(\frac{m_{23}e_3 - h_3}{zr_3}\right) \\
& + \tan^{-1}\left(\frac{m_{34}e_3 - h_3}{zr_3}\right) - \tan^{-1}\left(\frac{m_{34}e_4 - h_4}{zr_4}\right) \\
& \left. + \tan^{-1}\left(\frac{m_{41}e_4 - h_4}{zr_4}\right) - \tan^{-1}\left(\frac{m_{41}e_1 - h_1}{zr_1}\right) \right]
\end{aligned}
$$

(3.21)

In the above expression, instead of $|z|$ as reported in Katz and Plotkin (2001), only z is used. This modifies expression is found to be in good agree with the point source approximation as the distance between the field panel and source panel increases.

In the expressions (3.18), (3.19), (3.20) and (3.21) the intermediate terms are given by the below equations:

$$ d_{12} = \sqrt{(x_2 - x_1)^2 + (y_2 - y_1)^2} \tag{3.22} $$

$$ d_{23} = \sqrt{(x_3 - x_2)^2 + (y_3 - y_2)^2} \tag{3.23} $$

$$ d_{34} = \sqrt{(x_4 - x_3)^2 + (y_4 - y_3)^2} \tag{3.24} $$

$$ d_{41} = \sqrt{(x_1 - x_4)^2 + (y_1 - y_4)^2} \tag{3.25} $$

$$m_{12} = \frac{y_2 - y_1}{x_2 - x_1} \qquad (3.26)$$

$$m_{23} = \frac{y_3 - y_2}{x_3 - x_2} \qquad (3.27)$$

$$m_{34} = \frac{y_4 - y_3}{x_4 - x_3} \qquad (3.28)$$

$$m_{41} = \frac{y_1 - y_4}{x_1 - x_4} \qquad (3.29)$$

$$r_1 = \sqrt{(x - x_1)^2 + (y - y_1)^2 + z^2} \qquad (3.30)$$

$$r_2 = \sqrt{(x - x_2)^2 + (y - y_2)^2 + z^2} \qquad (3.31)$$

$$r_3 = \sqrt{(x - x_3)^2 + (y - y_3)^2 + z^2} \qquad (3.32)$$

$$r_4 = \sqrt{(x - x_4)^2 + (y - y_4)^2 + z^2} \qquad (3.33)$$

$$e_1 = z^2 + (x - x_1)^2 \qquad (3.34)$$

$$e_2 = z^2 + (x - x_2)^2 \qquad (3.35)$$

$$e_3 = z^2 + (x - x_3)^2 \qquad (3.36)$$

$$e_4 = z^2 + (x - x_4)^2 \qquad (3.37)$$

3.5 Frequency dependent part of Green function

The frequency dependent part of the green function $\tilde{G}(x, x_s, \omega_e)$ and its derivatives are evaluated using the numerical methods given in Telste and Noblesse (1986). The given expressions for derivatives and integrals are shown below :

$$\tilde{G}(\boldsymbol{x}, \boldsymbol{x_s}, \omega_e) = 2f\left[R_0(h, v) - i\pi J_0(h)e^v\right] \qquad (3.38)$$

$$\frac{\partial \tilde{G}_0}{\partial \rho_G} = -2f^2\left[R_1(h, v) - i\pi J_1(h)e^v\right] \qquad (3.39)$$

$$\frac{\partial \tilde{G}_0}{\partial x} = \frac{(x_P^e - x_Q^e)}{\rho_G}\frac{\partial \tilde{G}_0}{\partial \rho_G} \qquad (3.40)$$

$$\frac{\partial \tilde{G}_0}{\partial y} = \frac{\left(y_P^e - y_Q^e\right)}{\rho_G}\frac{\partial \tilde{G}_0}{\partial \rho_G} \qquad (3.41)$$

$$\frac{\partial \tilde{G}_0}{\partial z} = 2f^2\left[\frac{1}{d} + R_0(h, v) - i\pi J_0(h)e^v\right] \qquad (3.42)$$

where,

$$f = \frac{\omega^2 L}{g} \tag{3.43}$$

$$\rho_G = \left[(x_P^e - x_Q^e)^2 + (y_P^e - y_Q^e)^2\right]^{\frac{1}{2}} \tag{3.44}$$

$$r = \left[\rho_G^2 + (z_P^e - z_Q^e)^2\right]^{\frac{1}{2}} \tag{3.45}$$

$$r' = \left[\rho_G^2 + (z_P^e + z_Q^e)^2\right]^{\frac{1}{2}} \tag{3.46}$$

$$h = f\rho_G \tag{3.47}$$

$$v = f(z_P^e + z_Q^e) \tag{3.48}$$

$$d = fr' \tag{3.49}$$

where, J_0 and J_1 are the first-kind Bessel functions, L is a non-dimensionalizing length selected by the user, and g is the acceleration due to gravity. In this thesis $L = 1$ is used. Real valued functions $R_0(h, v)$ and $R_1(h, v)$ are effectively evaluated using the numerical method suggested by Telste and Noblesse (1986).

Once, the potentials are computed pressure can be obtained on each panel. Through integration of pressure throughout the submerged surface forces can be evaluated. Using radiation potentials added mass and radiation damping can be computed. After, obtaining all these coefficients and using them motion equation can be solved to get the RAOs. Steps to compute these forces and motion are explained in detail in the next section.

CHAPTER 4

FORCES and MOTIONS

4.1   Wave Potentials

Once the $[\alpha]$ matrix is computed using the expressions derived in the previous sections. Using the (3.8) we can solve for unknown source strength σ. Here, normal velocity vector $\{v_n\}$ matrix will be different for radiation and scattering potentials. It is computed by applying the boundary conditions given in the section(2.4). For $\{v_n\}$ related to scattering problem requires incident potential given by

$$\phi_I = \frac{igA}{\omega_I} \exp[-ik_I(x\cos\beta + y\sin\beta) + kz] \tag{4.1}$$

Note that, all the potentials are computed at the centroid of the panels. After applying respective boundary conditions for radiation and scattering problem unknown source strength can be calculated for the respective potentials / problems.

Once, the $[\beta]$ matrix is computed using the green function explained in section (3.3), combining it with respective source strength of radiation and scattering problems, using (3.1) respective potentials can be computed.

ϕ_D is used to denote scattering potential and $\phi_k (k = 1, 2, \cdots, 6)$ is used to denote the radiation potential in all 6-degrees of freedom. According to Salvesen *et al.* (1970) for radiation potential ϕ_k correction terms are added for 5th and 6th mode of motion.

$$\phi_j = \phi_j^0 \quad \text{for} j = 1, 2, 3, 4 \tag{4.2}$$
$$\phi_5 = \phi_5 + \frac{U}{i\omega_e}\phi_3^0$$
$$\phi_6 = \phi_6^0 - \frac{U}{i\omega_e}\phi_2^0$$

ϕ_j^0 are the zero speed terms computed without the effect forward speed, method to compute these quantities is given in Guha (2012). But, there is a slight change while computing the zero speed terms given in the cited paper, for boundary condition used in forward speed is considered which is the boundary condition given in 2.4. Then after, to the obtained radiation potentials with forward speed effect, for 5th and 6th mode of motions extra correction terms are added according to Salvesen *et al.* (1970). Once, the radiation potential is computed added mass and radiation damping can be obtained using its acceleration and velocity components.

4.2   Exciting forces

Once all potentials are computed, through direct integration on the submerged surface forces can be computed. **Froude Krylov force** is calculated using incident wave potential given in eq.(4.1). Hence, equation for Froude Krylov force / incident force for modes $(k = 1, 2, \cdots, 6)$ is

$$F_I^k = -\iota\omega \int_S \phi_I n_k ds \tag{4.3}$$

Similar to Froude Krylov force, **Scattering force** is obtained through integration of scattering force over the submerged surface. Hence, for all modes $(k = 1, 2, \cdots, 6)$ equation for scattering force is

$$
\begin{aligned}
\boldsymbol{F}_D^k &= \rho \int_S (\iota\omega_e n_k - U m_k)\phi_D \, ds \tag{4.4} \\
&= -\rho \int_S \phi_k^0 \frac{\partial \phi_I}{\partial n} ds \quad \text{for} k = 1, 2, 3, 4 \\
&= -\rho \int_S \phi_k^0 \frac{\partial \phi_I}{d} s + \frac{\rho U}{i\omega_e} \int_S \phi_3^0 \frac{\partial \phi_I}{d} s \quad \text{for} k = 5 \\
&= -\rho \int_S \phi_k^0 \frac{\partial \phi_I}{d} s - \frac{\rho U}{i\omega_e} \int_S \phi_2^0 \frac{\partial \phi_I}{d} s \quad \text{for} k = 6
\end{aligned}
$$

Now, the total **exciting force** amplitude (Fourde Krylov + Scattering) in mode $(k = 1, 2, \cdots 6)$ is given by

$$\boldsymbol{F} = \boldsymbol{F}_I^k + \boldsymbol{F}_D^k \tag{4.5}$$

4.3 Radiation forces

Radiation wave loads due to the waves created by the movement of the body in fluid. Equation for wave load for all modes of motion $(k = 1, 2, \cdots, 6)$ is given by

$$F_R^k = -\iota\omega_e\rho \int_S \phi_k n_k ds \tag{4.6}$$

$$= \omega_e^2 A_{jk} - \iota\omega_e B_{jk}$$

In the expansion of above equation there are two terms, the term proportional to the acceleration is added mass and the one proportional to the velocity is radiation damping. Equations for added mass and radiation damping is given as

$$A_{jk} = -\frac{\rho}{\omega_e} \int_S \text{Im}(\phi_k) n_j ds \tag{4.7}$$

$$B_{jk} = -\rho \int_S \text{Re}(\phi_k) n_j ds \tag{4.8}$$

Note, that Added mass A_{jk} and Radiation damping B_{jk} are real valued. Also the subscript (jk) denotes the added mass or radiation damping in j^{th} mode of motion due to the body oscillation along the kth direction.

4.3.1 Forward speed RAO

For a regular incident wave of unit amplitude the steady state motion $\{\eta\} = \eta_a e^{\omega t}$ is governed by :

$$-\omega^2[M + A]\{\eta\} + i\omega[B]\{\eta\} + [C]\{\eta\} = \{F\} \tag{4.9}$$

where, $[M]$ is the mass matrix, $[A]$ is the added mass matrix, $[B]$ denotes the radiation damping matrix, $[C]$ denotes the stiffness matrix, $\{F\}$ denotes the external force vector which is Exciting force (Froude Kerlov force + Scattering force) and $\{\eta_a\}$ denotes the amplitude of steady state motion.

Hence, the response amplitude operator **RAO** $\{\eta\}$ is given by

$$\{\eta\} = \frac{\{F\}}{(-\omega^2[M+A]+i\omega[B]+[C])} \tag{4.10}$$

CHAPTER 5

DRIFT FORCES

5.1 Introduction

Mean drift forces are the mean non-linear forces which can be obtained using perturbation theory. Forces explained and computed in the previous chapters are first order forces. While solving boundary value problems to get the potential, pressure, forces, motions, etc. usually second order terms are ignored in order to reduce the complexity of the problem and also the mangitude of second order terms which are these mean forces is also very small. But when the actual responses are very high, these second order mean forces become important. These forces are proportional to swuare of the wave height while the first order are proportional to the wave height. Primarily, mean drift forces are computed using two menthods: (a) far field method and (b) near field method.

This chapter deals with the mean drift force and moments acting on a stationary vessel in regular waves. This chapter presents the complete derivation of the second order force on an arbitrary shaped body moving with a steady forward speed in regular waves using 3D panel based potential theory. Far field method introduced by Maruo (1957) is based on the diffracted and radiated wave energy and momentum flux at infinity. Near feild method introduced by Boese (1970) uses direct hydrodynamic pressure integration over the wetted surface and is based on 3D panel based potential theory.

Lastly, comparisons between MDLhydroD and WAMIT6 is shown in the results section (6.3). MDLHydroD considers the effect of hull emergence angle, hence the drift force is considerably less compared to WAMIT6. Due to time constraints, the code was not implemented into the HydRA program. Comparisons of different software alone is done.

5.2 Perturbation expansions

Perturbation theory is used to obtain the approximation solution upto a certain accuracy. Solution or quantity is expressed as a power series using a small parameter known as perturbation parameter. Perturbation expressions start with an average solution. For example,

$$A = A_0 + \epsilon A_1 + \epsilon^2 A_2 + \cdots \tag{5.1}$$

where, ϵ is the perturbation parameter and A_0 is the average solution of A.

Now, Assuming small amplitude motion oscillations about mean position of the body, approximations can be obtain up to second order with respect to the wave amplitude. Perturbation expressions of quantities of interest using a small parameter ϵ of the order of the wave slope, are given below :

1. Expressions for velocity potential $(\phi = \phi_T \, e^{i \, w_e \, t})$:

$$\phi = \epsilon \phi^{(1)} + \epsilon^2 \phi^{(2)} + \cdots \tag{5.2}$$

2. The free surface elevation (ζ) :

$$\zeta = \epsilon \zeta^{(1)} + \epsilon^2 \zeta^{(2)} + \cdots \tag{5.3}$$

3. The relative wave elevation:

$$\zeta_r = \epsilon \zeta_r^{(1)} + \epsilon^2 \zeta_r^{(2)} + \cdots \tag{5.4}$$

4. The vessel motions :

$$\vec{\eta}(t) = \epsilon \vec{\eta}^{(1)} + \epsilon^2 \vec{\eta}^{(1)} + \cdots \tag{5.5}$$

   where, $\vec{\eta}^{(1)} = (\eta_1, \eta_2, \eta_3, \eta_4, \eta_5, \eta_6)$ represents the first order surge, sway, heave, roll, pitch and yaw motions respectively.

5. The pressure field in the fluid :

$$p = p^{(0)} + \epsilon p^{(1)} + \epsilon^{2(2)} + \cdots \tag{5.6}$$

5.3 Pressure and force derivations

5.3.1 Pressure derivation

The pressure using Bernoulli's equation is given as:

$$p = \frac{1}{2}\rho\, U^2 - \rho\frac{\partial\phi_T}{\partial t} - \frac{1}{2}\rho|\nabla\phi_T| - \rho\, g\, z^2 \tag{5.7}$$

After substituting the above expression in (5.6), pressure quantities with respect to zeroth order of ϵ are given as

$$p^{(0)} = -\rho g(z_B + z_0) \tag{5.8}$$

where, $(\vec{X_0}) = (X_0, Y_0, Z_0)$ is the location of body coordinate system origin with respect to the global coordinate system and $\vec{x_B} = (x_B, y_B, z_B)$ the location of the point where the quantity is being computed in the body coordinate system. First and second order expression for pressure is given as:

$$p^{(1)} = -\rho g z^{(1)} - \rho\frac{\partial\phi^{(1)}}{\partial t} + +\rho U\frac{\partial\phi^{(1)}}{\partial x} \tag{5.9}$$

$$P^{(2)} = -\rho\frac{\partial\phi^{(2)}}{\partial t} + \rho U\frac{\partial\phi^{(2)}}{\partial x} - \frac{\rho}{2}\left\{\left(\frac{\partial\phi^{(1)}}{\partial x}\right)^2 + \left(\frac{\partial\phi^{(1)}}{\partial y}\right)^2 + \left(\frac{\partial\phi^{(1)}}{\partial z}\right)^2\right\}$$

$$\tag{5.10}$$

$$- \rho\left\{x^{(1)}\cdot\nabla\left(\frac{\partial\phi^{(1)}}{\partial t} - U\frac{\partial\phi}{\partial x}\right)\right\} - \rho g z^{(2)}$$

where, $z^{(2)} = [\eta_4\eta_6 x_B + \eta_5\eta_6 y_B - \frac{1}{2}(\eta_4^2 + \eta_5^2)z_B]$. All the potentails and their derivatives are calculated at mean position.

5.3.2 Relative wave elevation

Relative wave elevation is the distance between the wave surface and the instantaneous waterline. To calculate the relative wave elevation, first absolute wave elevation needs to be calculated along the waterline. The waterline is obtained by extracting the edges of the panels which are at the water surface. According to the dynamic free surface boundary condition the pressure at free surface is zero (gauge pressure) i.e. at $\zeta = 0$, $p = 0$. Hence,

$$\rho g \zeta + \rho \frac{\partial \phi}{\partial t} - \rho U \frac{\partial \phi}{\partial x} = 0 \quad \text{on} \quad z = \zeta \tag{5.11}$$

Therefore the above equation yields :

$$\zeta^{(1)} = -\frac{1}{g} \left(i\omega_e \phi_T - U \frac{\partial \phi_T}{\partial x} \right) e^{i\,\omega_e\,t} \tag{5.12}$$

The relative wave elevation is then obtained by subtracting the total movement of the body in z-direction from the absolute wave elevation.

$$\zeta_r^{(1)} = \zeta^{(1)} - (\eta_3 - \eta_5 x + \eta_4 y) \tag{5.13}$$

where, (x, y) are the centroid of the waterline panels or the waterline element.

5.3.3 Forces and moments

Hydrodynamic force is obtained by integrating the pressure over the wetter surface or submerged surface of the vessel. Now, hydrodynamic force and moment is given by is given as

$$\vec{F} = -\int_S P\,\hat{n}_j\,ds \qquad j = 1, 2, \cdots, 6 \tag{5.14}$$

$$\vec{M} = -\int_S P\,(\vec{x} \times \hat{n}_j)\,dS \tag{5.15}$$

Using the perturbation expansions till second degree, equations for force can be written as

$$\vec{F} = -\left(\int_{S_0} ds + \int_{wl} \zeta_r dl\right)(p^{(0)} + \epsilon p^{(1)} + \epsilon^2 p^{(2)})(\vec{n}^{(0)} + \epsilon(\vec{\theta}^{(0)} \times \vec{n}^{(0)}) + \epsilon^2 H\vec{n}^{(0)})$$

(5.16)

The waterline integral arises due to the consideration of the first order wetted surface area S_1 which is the additional instantaneous surface of the hull below water considering both wave elevation and the motion of the body.

$$\int_{S_1} \cdots ds = \int_{wl} dl \int_0^{\zeta_r} \cdots \frac{dz}{\sqrt{1 - n_3^2}}$$

(5.17)

Here, wl is the waterline of the ship, ζ_r is the relative wave elevation and according to Guha and Falzarano (2015a), $dz/\sqrt{1 - n_3^2}$ is the inclined height for non-wall sided surface. In the equation (5.16), matrix H represents the second order rotation matrix given as:

$$H = \begin{bmatrix} -\frac{1}{2}(\eta_5^2 + \eta_6^2) & 0 & 0 \\ \eta_4\eta_5 & -\frac{1}{2}(\eta_4^2 + \eta_6^2) & 0 \\ \eta_4\eta_6 & \eta_5\eta_6 & -\frac{1}{2}(\eta_4^2 + \eta_5^2) \end{bmatrix}$$

(5.18)

Expanding (5.16) and separating the terms corresponding to ϵ, ϵ^1 and ϵ^2 gives the zeroth, first and second order force respectively.

$$\vec{F}^{(0)} = -\int_{S_0} p^{(0)}\vec{n}^{(0)} ds$$

(5.19)

$$\vec{F}^{(1)} = -\int_{S_0} p^{(0)}(\vec{\theta}^{(1)} \times \vec{n}^0) ds - \int_{S_0} p^{(1)}\vec{n}^{(0)} ds - \int_{wl} \zeta_r^{(1)} p^{(0)}\vec{n}^{(0)} dl$$

(5.20)

$$\vec{F}^{(2)} = -\int_{S_0} p^{(0)}(H \vec{n}^0) ds - \int_{S_0} p^{(1)}(\vec{\theta}^{(1)} \times \vec{n}^{(0)}) ds - \int_{S_0} p^{(2)}\vec{n}^{(0)} ds$$
$$- \int_{wl} \zeta_r^{(1)}(\vec{\theta}^{(1)} \times \vec{n}^{(0)}) dl - \int_{wl} \zeta_r^{(1)} p^{(1)}\vec{n}^{(0)} dl - \int_{wl} \zeta_r^{(2)} p^{(0)}\vec{n}^{(0)} dl$$

(5.21)

Now, substituting relative wave elevation (5.13) and pressure equations which are (5.7), (5.9) in (5.21) and extracting terms corresponding to ϵ^2 second order force can be obtained whose equation is given below :

$$
\begin{aligned}
\vec{F}^{(2)} = & -\int_{wl} \frac{1}{2}\rho g(\zeta_r^{(1)})^2 \frac{\vec{n}^{(0)}}{\sqrt{1-n_3^2}}dl + \int_{S_0} \rho\left(\frac{\partial\phi^{(2)}}{\partial t} - U\frac{\partial\phi^{(2)}}{\partial x}\right)\vec{n}^{(0)}ds \quad (5.22) \\
& + \int_{S_0} \frac{\rho}{2}\left\{\left(\frac{\partial\phi^{(1)}}{\partial x}\right)^2 + \left(\frac{\partial\phi^{(1)}}{\partial x}\right)^2 + \left(\frac{\partial\phi^{(1)}}{\partial x}\right)^2\right\}\vec{n}^{(0)}\,ds \\
& + \int_{S_0} i\omega_e\rho\left\{(\eta_1 - \eta_6 y_B + \eta_5 z_B)\frac{\partial\phi^{(1)}}{\partial x}\right. \\
& \left. +(\eta_2 + \eta_6 x_B - \eta_4 z_B)\frac{\partial\phi^{(1)}}{\partial y} + (\eta_3 - \eta_5 x_B + \eta_4 y_B)\frac{\partial\phi^{(1)}}{\partial z}\right\}\vec{n}^{(0)}\,ds \\
& - \rho g A^{(0)}\left[\eta_4\eta_6 x_{B,f} + \eta_5\eta_6 y_{B,f} + \frac{1}{2}(\eta_4^2 + \eta_5^2)Z_0\right]\hat{k} \\
& - \omega_e^2\{-\eta_2\eta_6 m + \eta_4\eta_6 mz_g - \eta_6\eta_6 mx_g + \eta_3\eta_5 m + \eta_4\eta_5 y_g - \eta_5\eta_5 mx_g\}\hat{i} \\
& - \omega_e^2\{\eta_1\eta_6 m + \eta_5\eta_6 mz_g - \eta_6\eta_6 my_g - \eta_3\eta_4 m + \eta_4\eta_4 my_g + \eta_4\eta_5 mx_g\}\hat{j} \\
& - \omega_e^2\{-\eta_1\eta_5 m - \eta_5\eta_5 mz_g + \eta_5\eta_6 my_g + \eta_2\eta_4 m - \eta_4\eta_4 mz_g + \eta_4\eta_6 mx_g\}\hat{k}
\end{aligned}
$$

Similarly, the second order moment can be given as :

$$\vec{M}^{(2)} = -\int_{wl} \frac{1}{2}\rho g(\zeta_r^{(1)})^2(x_B \times \vec{n}^{(0)})dl \tag{5.23}$$

$$+ \rho\int_{S_0}\left(\frac{\partial\phi^{(2)}}{\partial t} - U\frac{\partial\phi^{(2)}}{\partial x}\right)(\vec{x_B} \times \vec{n}^{(0)})\,ds$$

$$+ \frac{\rho}{2}\int_{S_0}\left\{\left(\frac{\partial\phi^{(1)}}{\partial x}\right)^2\left(\frac{\partial\phi^{(1)}}{\partial y}\right)^2 + \left(\frac{\partial\phi^{(1)}}{\partial z}\right)^2\right\}(\vec{x_B} \times \vec{n}^{(0)})\,ds$$

$$+ i\omega_e\rho\int_{S_0}\left\{(\eta_1 - \eta_6 y_B + \eta_5 z_B)\frac{\phi^{(1)}}{\partial x}\right.$$

$$+(\eta_2 - \eta_6 x_B - \eta_4 z_B)\frac{\phi^{(1)}}{\partial y}$$

$$\left.+(\eta_3 - \eta_5 x_B + \eta_4 y_B)\frac{\phi^{(1)}}{\partial z}\right\}(\vec{x_B} \times \vec{n}^{(0)})\,ds$$

$$- \omega_e^2\{\eta_2\eta_4 my_g - \eta_1\eta_6 mz_g - \eta_4\eta_6 I_{54} - eta_5\eta_6 I_{55} - \eta_6\eta_6 I_{56}$$

$$+ \eta_3\eta_4 mz_g - \eta_1\eta_5 my_g + \eta_4\eta_5 I_{64} + \eta_5\eta_5 I_{65} + \eta_5\eta_6 I_{66}\}\hat{i}$$

$$- \omega_e^2\{\eta_3\eta_5 mz_g - \eta_2\eta_6 mz_g + \eta_4\eta_6 I_{44} + \eta_5\eta_6 I_{45} + \eta_6\eta_6 I_{46}$$

$$+ \eta_1\eta_5 mx_g - \eta_2\eta_4 mx_g - \eta_4\eta_4 I_{64} - \eta_4\eta_5 I_{65} - \eta_4\eta_6 I_{66}\}\hat{j}$$

$$- \omega_e^2\{\eta_1\eta_6 mx_g - \eta_3\eta_5 my_g - \eta_4\eta_5 my_g - \eta_4\eta_5 I_{44} - \eta_5\eta_5 I_{45} - \eta_5\eta_6 I_{46}$$

$$+ \eta_2\eta_6 my_g - \eta_3\eta_4 mx_g + \eta_4\eta_4 I_{54} + \eta_4\eta_4 I_{55} + \eta_4\eta_6 I_{56}\}\hat{k}$$

$$+ \rho g\left[-V^{(0)}\eta_1\eta_6 + V^{(0)}\eta_4\eta_5 x_{CB} - V^{(0)}\eta_5\eta_6 z_{CB} - \frac{1}{2}V^{(0)}(\eta_4^2 - \eta_6^2)y_{CB}\right.$$

$$\left.-\eta_4\eta_6 L_{12} - \eta_5\eta_6 L^{22} - \frac{1}{2}(\eta_4^2 + \eta_5^2)Z_0 A^{(0)}y_f + \eta_5\eta_6 V^{(0)}Z^{(0)}\right]\hat{i}$$

$$+ \rho g\left[-V^{(0)}\eta_2\eta_6 + V^{(0)}\eta_4\eta_6 z_{CB} + \frac{1}{2}V^{(0)}(n\eta - 5^2 - \eta_6^2)x_{CB}\right.$$

$$\left.+\eta_4\eta_6 L_{11} + \eta_5\eta_6 L_{12} + \frac{1}{2}(\eta_4^2 + \eta_5^2)Z_0 A^{(0)}x_f - \eta_4\eta_6 Z_0 V^{(0)}\right]\hat{j}$$

$$+ \rho g V^{(0)}(\eta_1\eta_4 + \eta_2\eta_5 + \eta_5\eta_6 x_{CB} - \eta_4\eta_6 y_{CB})\hat{k}$$

CHAPTER 6

RESULTS AND DISCUSSION

The outputs of developed program **HydRA** are compared against the outputs of the software MDLHydroD. For comparison KCS and KVLCC2 vessels' hull structure is used.

6.1 Forward speed comparisons for KCS Vessel

KCS (Krisco container ship) is a fine form container ship and its particulars are listed in Table 6.1. For comparison, frequencies are used from -0.03 with $+0.03$ increment and in total 34 frequencies are used. Here, -ve frequency is used to simulate the effect of infinite frequency case and while plotting the comparisons zero and -ve frequencies are ignored. Ship's speed is $8\,\mathrm{m\,s^{-1}}$. Incident angles used ranges from $0°$ to $345°$ with $15°$ increment. Simulation was ran for 6 modes of motion. The comparison of added mass for different angles are shown in figure 6.1. Comparisons of radiation damping is shown in figure 6.2. Comparisons of Froude Krylov force is shown in figure 6.3. Comparisons of Scattering force is shown in figure 6.4. Comparisons of RAO is shown in figure 6.5 and figure 6.6

Table 6.1: KCS principal particulars

Main Particulars	Value
Length between perpendiculars L (m)	230
Breadth B (m)	32.2
Draft d (m)	10.8
Displacement ∇ (m^3)	52030
Block coefficient C_b	0.651
Radius of Gyration R_{zz}/L	0.25
Metacentric height GM (m)	1.20
LCB (% of L from midship, forward +ve)	-1.48%

6.1.1 Added mass

(a) $A_{22}\,\beta = 120°$

(b) $A_{22}\,\beta = 120°$

(c) $A_{11}\,\beta = 120°$

(d) $A_{22}\,\beta = 120°$

(e) $A_{22}\,\beta = 120°$

(f) $A_{22}\,\beta = 120°$
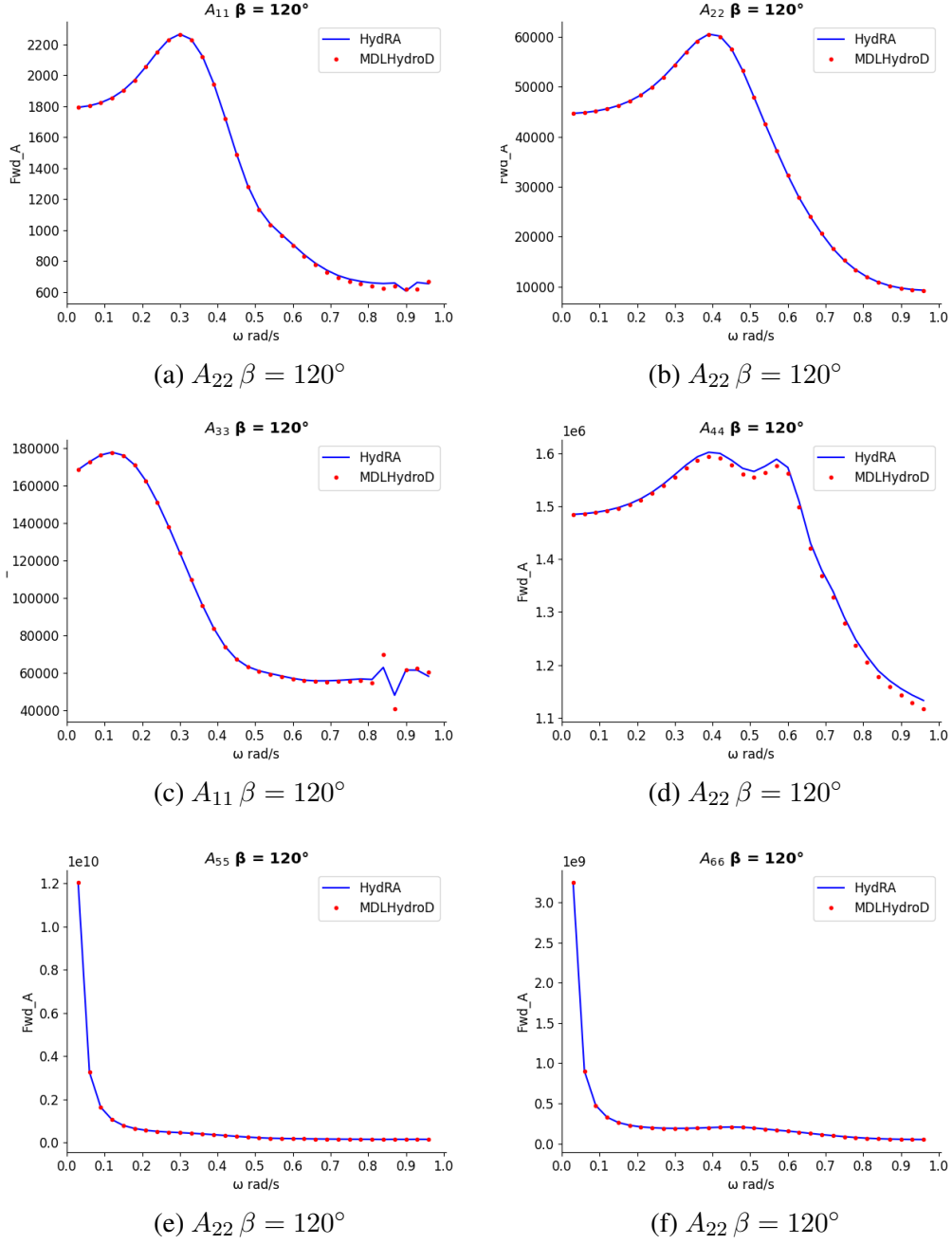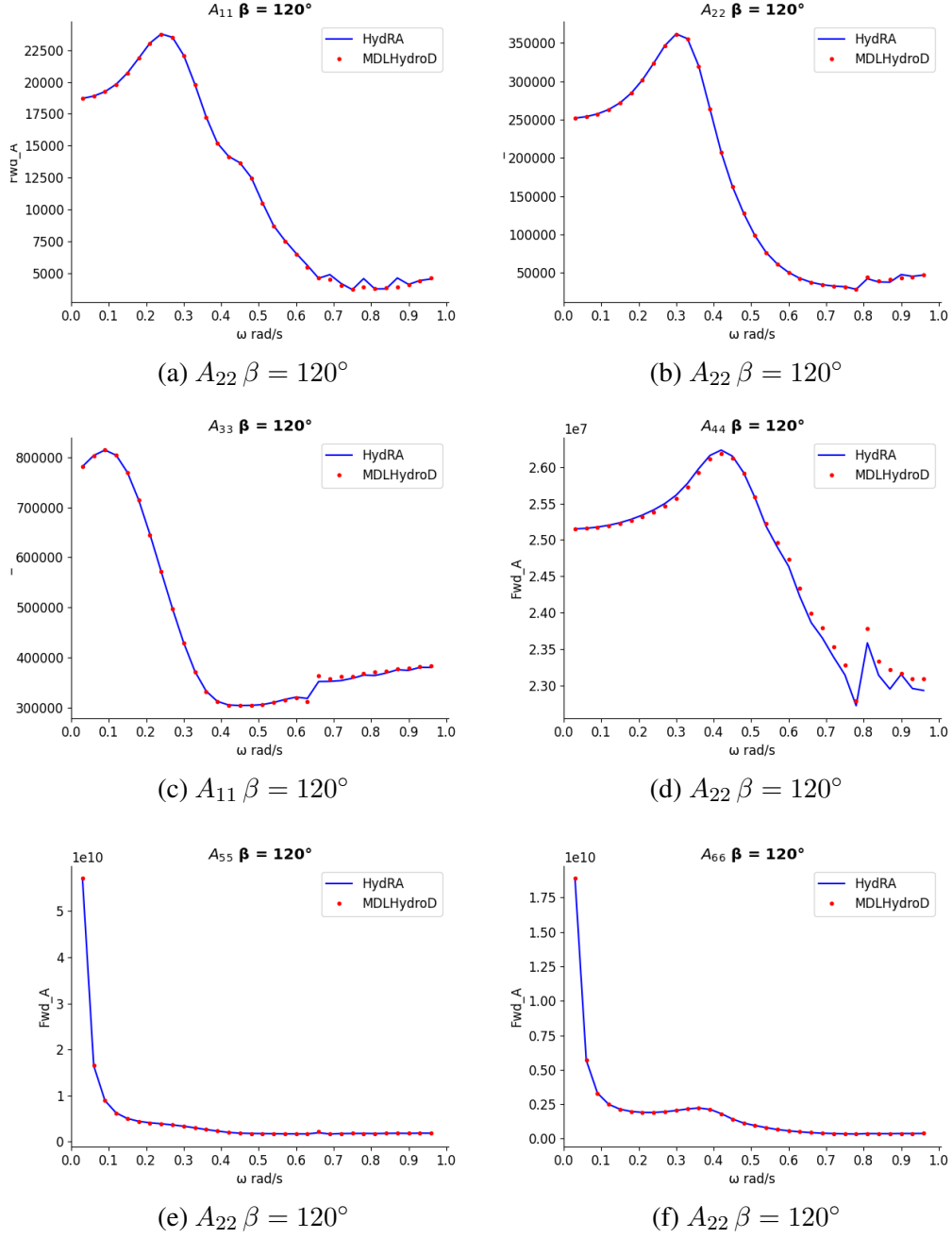
Figure 6.1: KCS vessel added mass comparison for $\beta = 120°$

6.1.2 Radiation damping

(a) B_{11} $\beta = 105°$

(b) B_{22} $\beta = 105°$

(c) B_{33} $\beta = 105°$

(d) B_{44} $\beta = 105°$

(e) B_{55} $\beta = 105°$

(f) B_{66} $\beta = 105°$
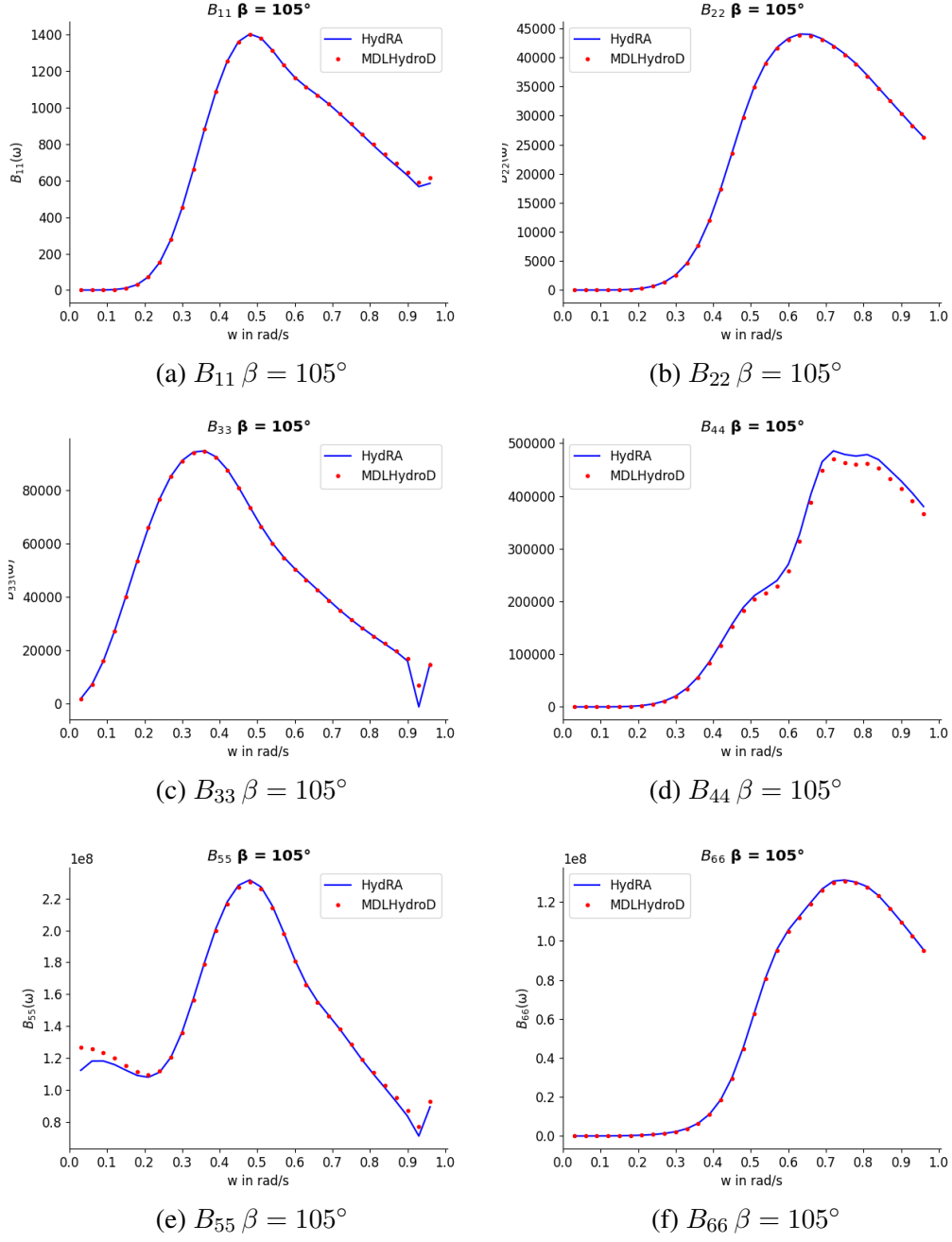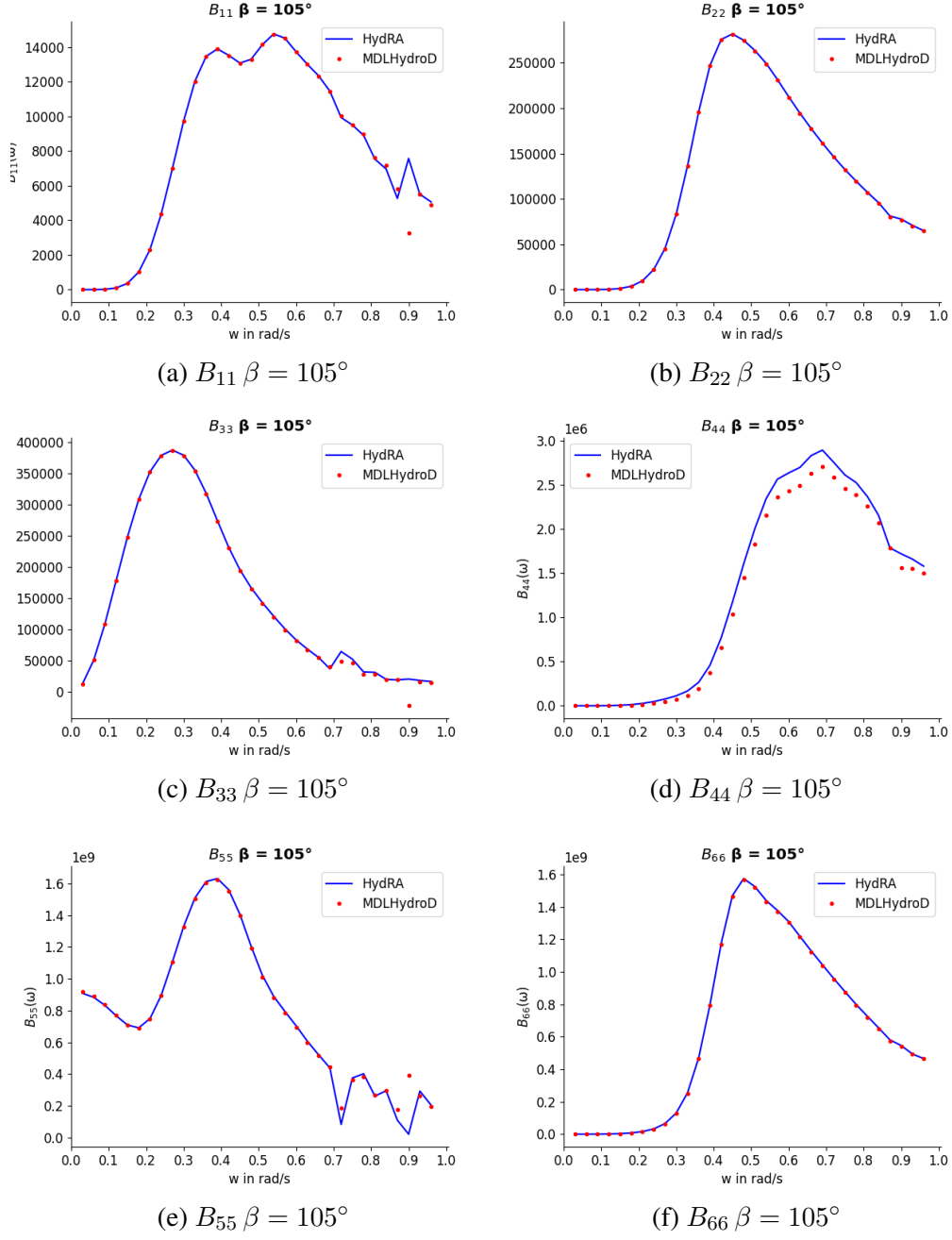
Figure 6.2: KCS vessel radiation damping comparison for $\beta = 105°$

6.1.3 Froude Krylov Force
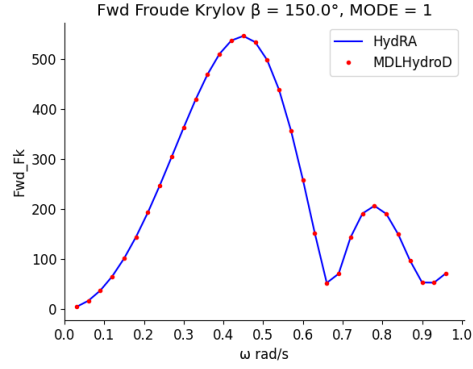
(a) Surge FkFrc $\beta = 150°$
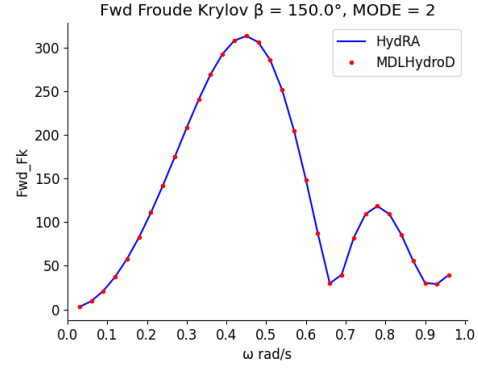
(b) Sway FkFrc $\beta = 150°$
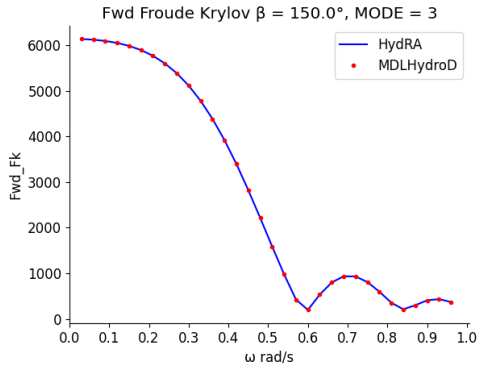
(c) Heave FkFrc $\beta = 150°$
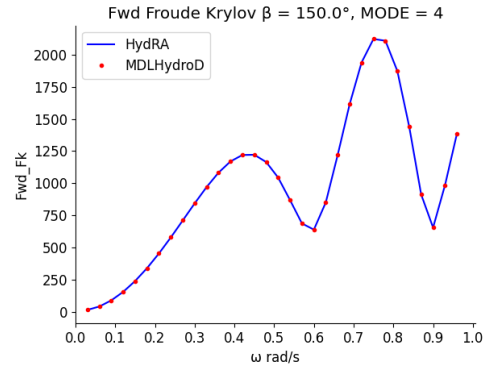
(d) Roll FkFrc $\beta = 150°$
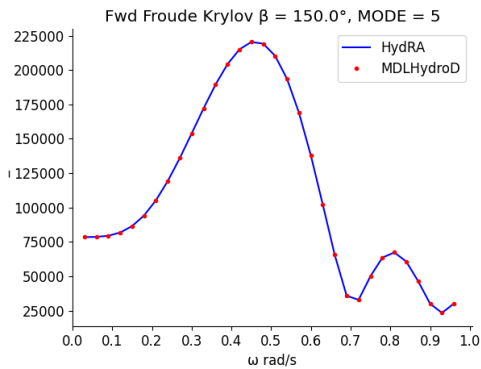
(e) Pitch FkFrc $\beta = 150°$
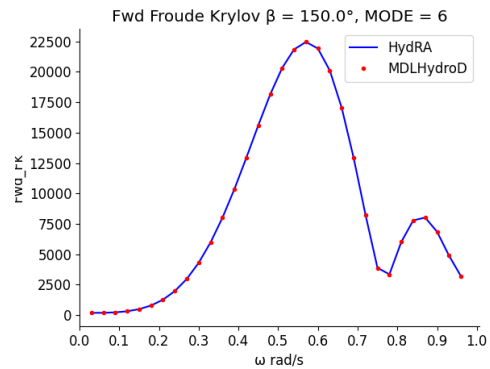
(f) Yaw FkFrc $\beta = 150°$

Figure 6.3: KCS vessel froude krylov force comparison for $\beta = 150°$

6.1.4 Scattering Force
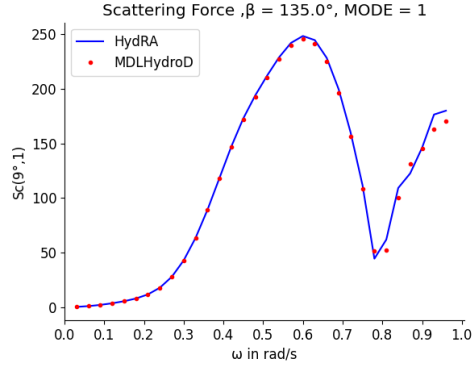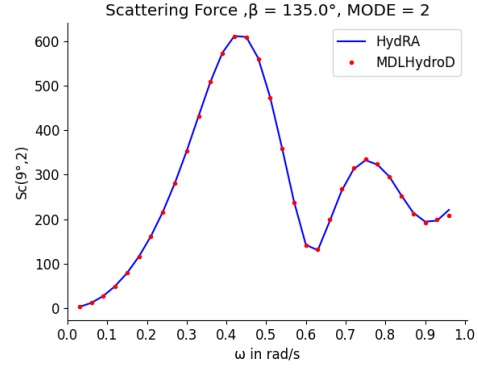
(a) Surge ScFrc $\beta = 135°$
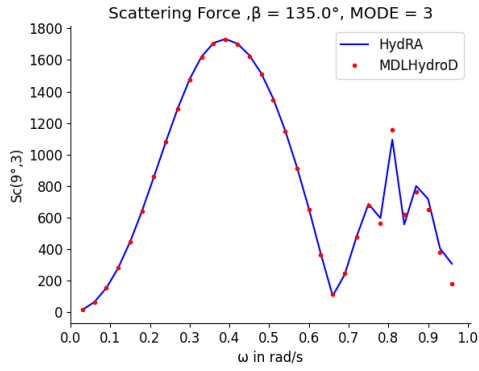
(b) Sway ScFrc $\beta = 135°$
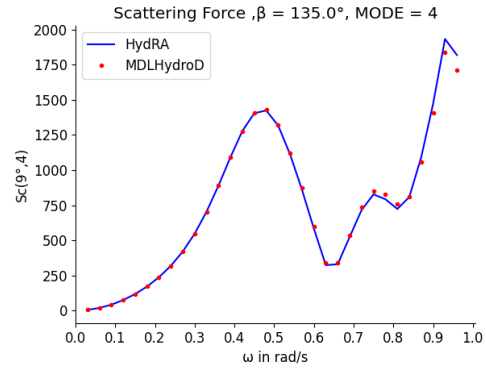
(c) Heave ScFrc $\beta = 135°$
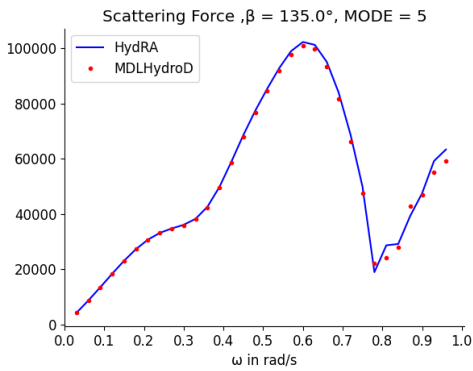
(d) Roll ScFrc $\beta = 135°$
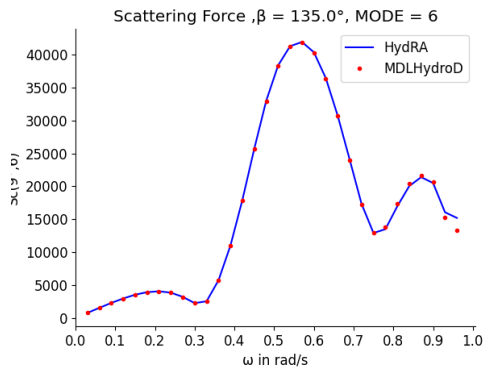
(e) Pitch ScFrc $\beta = 135°$

(f) Yaw ScFrc $\beta = 135°$

Figure 6.4: KCS vessel Scattering force comparison for $\beta = 135°$

6.1.5 RAO
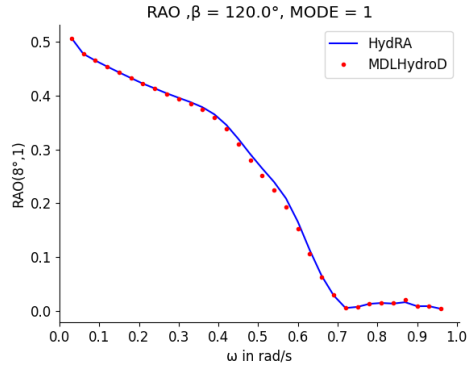
(a) Surge RAO $\beta = 120°$
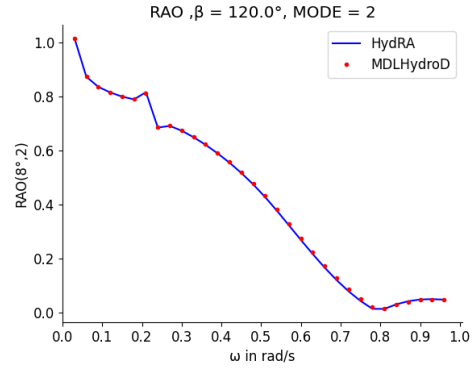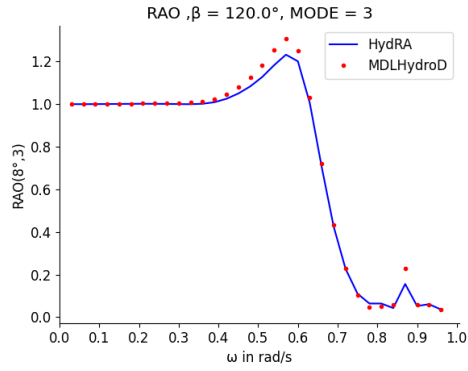
(b) Sway RAO $\beta = 120°$
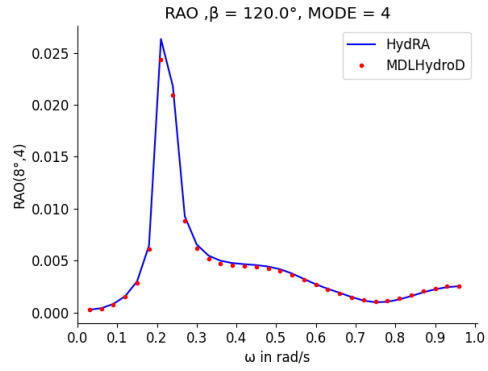
(c) Heave RAO $\beta = 120°$
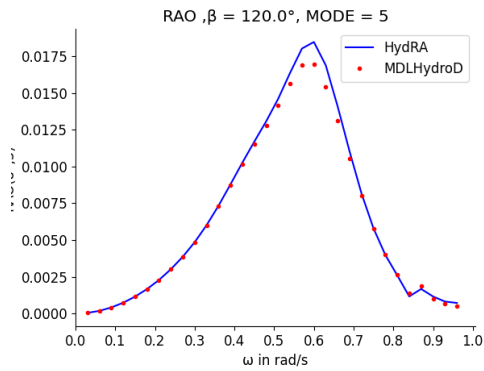
(d) Roll RAO $\beta = 120°$
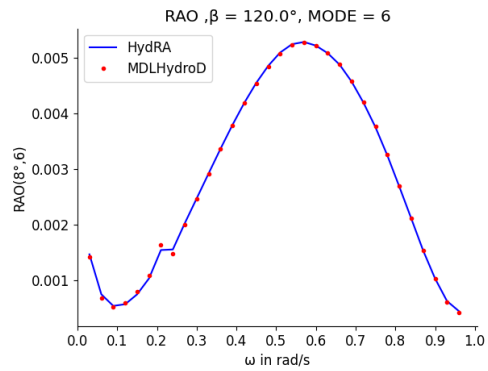
(e) Pitch RAO $\beta = 120°$

(f) Yaw RAO $\beta = 120°$

Figure 6.5: KCS vessel RAO comparison for $\beta = 120°$
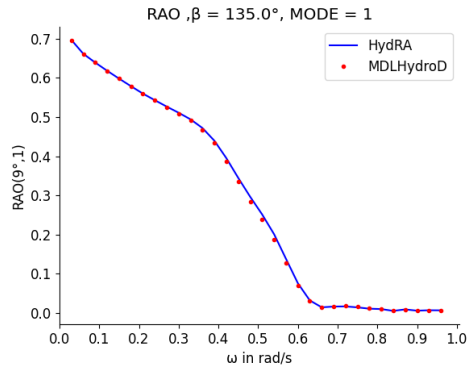
(a) Surge RAO $\beta = 135°$
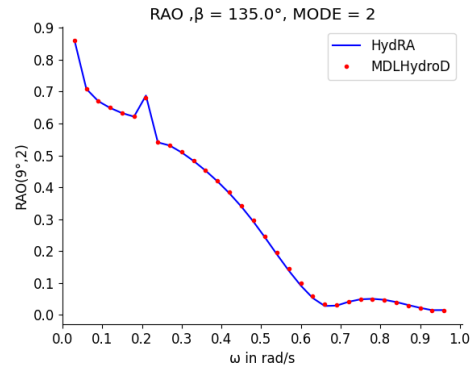
(b) Sway RAO $\beta = 135°$
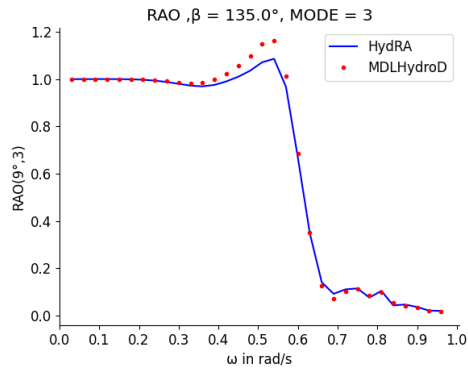
(c) Heave RAO $\beta = 135°$
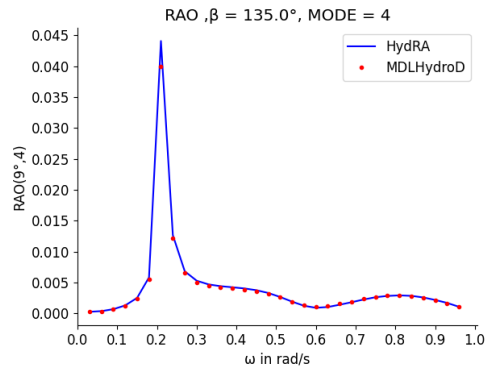
(d) Roll RAO $\beta = 135°$
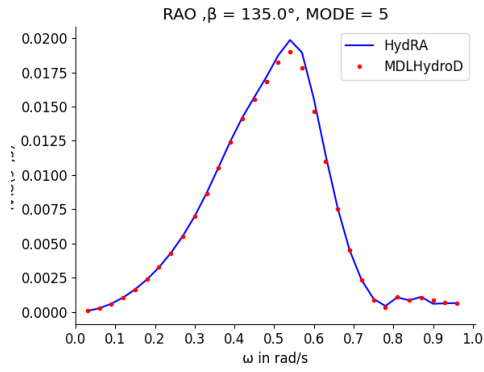
(e) Pitch RAO $\beta = 135°$
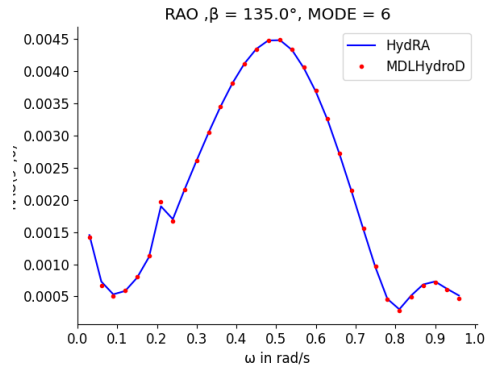
(f) Yaw RAO $\beta = 135°$

Figure 6.6: KCS vessel RAO comparison for $\beta = 135°$

6.2　Forward speed comparisons for KVLCC Vessel

Principle perticulars for KVLCC2 (Oil tanker) are given in the table **??**. For comparison, frequencies are used from -0.03 with $+0.03$ increment and in total 34 frequencies are used. Here, -ve frequency is used to simulate the effect of infinite frequency case and while plotting the comparisons zero and -ve frequencies are ignored. Ship's speed is $8\,\mathrm{m\,s^{-1}}$. Incident angles used ranges from $0°$ to $345°$ with $15°$ increment. Simulation is ran for all 6 modes of motion. The comparison of added mass for different angles are shown in figure 6.7. Comparisons of radiation damping is shown in figure 6.8. Comparisons of Froude Krylov force is shown in figure 6.9. Comparisons of Scattering force is shown in figure 6.10. Comparisons of RAO is shown in figure 6.5 and figure 6.12

Table 6.2: KVLCC2 principal particulars

Main Particulars	Value
Length between perpendiculars L (m)	320
Breadth B (m)	58
Draft d (m)	20.8
Displacement ∇ (m^3)	312622
Block coefficient C_b	0.8098
Radius of Gyration R_{zz}/L	0.25
Metacentric height GM (m)	5.71
LCB (% of L from midship, forward +ve)	3.48%

6.2.1 Added mass

(a) $A_{22}\,\beta = 120°$

(b) $A_{22}\,\beta = 120°$

(c) $A_{11}\,\beta = 120°$

(d) $A_{22}\,\beta = 120°$

(e) $A_{22}\,\beta = 120°$

(f) $A_{22}\,\beta = 120°$

Figure 6.7: KVLCC2 vessel added mass comparison for $\beta = 120°$

6.2.2 Radiation damping

(a) $B_{11}\, \beta = 105°$

(b) $B_{22}\, \beta = 105°$

(c) $B_{33}\, \beta = 105°$

(d) $B_{44}\, \beta = 105°$

(e) $B_{55}\, \beta = 105°$

(f) $B_{66}\, \beta = 105°$

Figure 6.8: KVLCC2 vessel radiation damping comparison for $\beta = 105°$

6.2.3 Froude krylov force
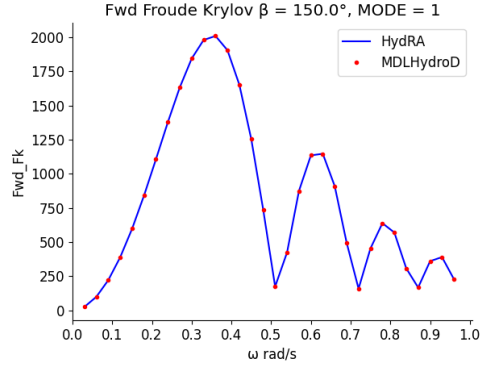
(a) $Fk\,\beta = 150°$
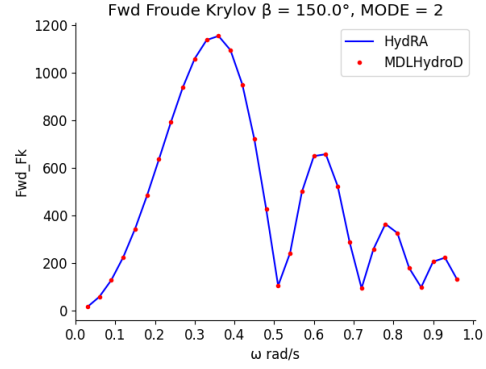
(b) $Fk\,\beta = 150°$
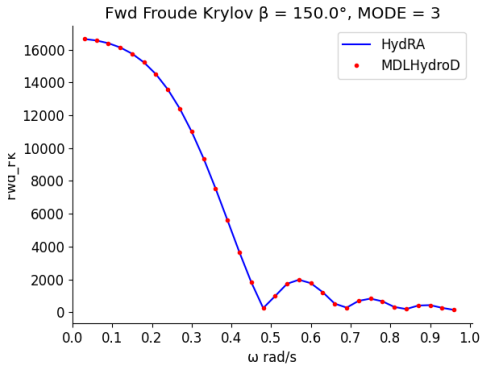
(c) $Fk\,\beta = 150°$
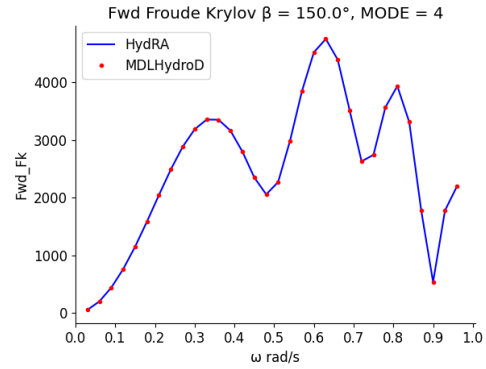
(d) $Fk\,\beta = 150°$
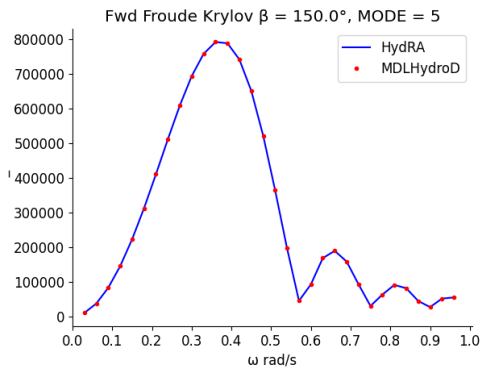
(e) $Fk\,\beta = 150°$
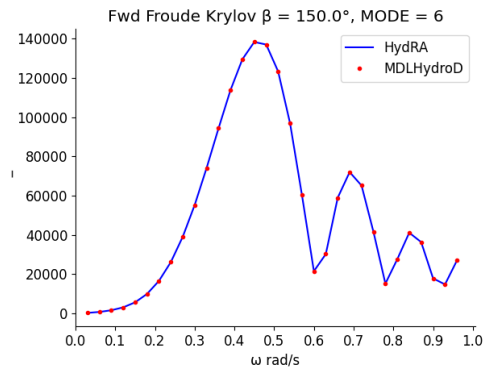
(f) $Fk\,\beta = 150°$

Figure 6.9: KVLCC2 vessel froude krylov force comparison for $\beta = 150°$

6.2.4 Scattering force
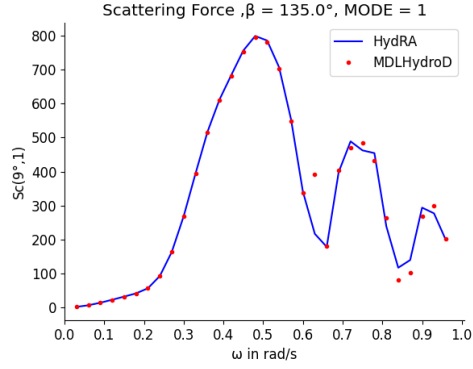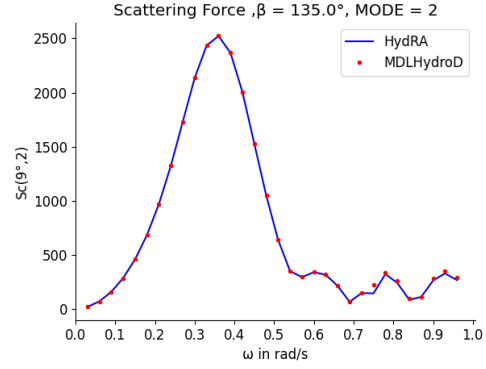
(a) Surge ScFrc $\beta = 135°$
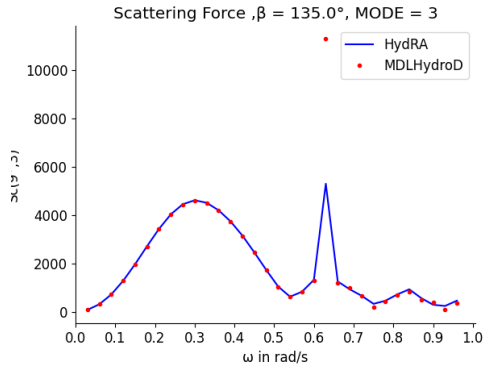
(b) Sway ScFrc $\beta = 135°$
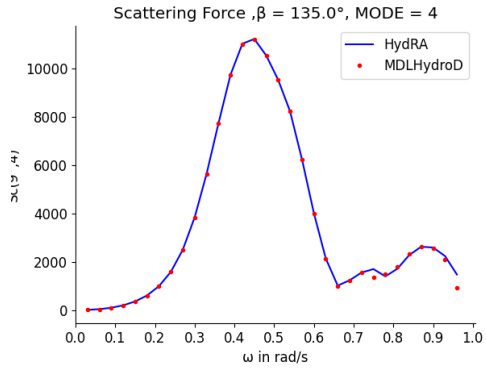
(c) Heave ScFrc $\beta = 135°$
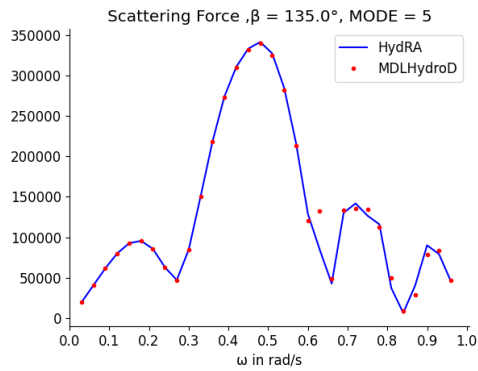
(d) Roll ScFrc $\beta = 135°$
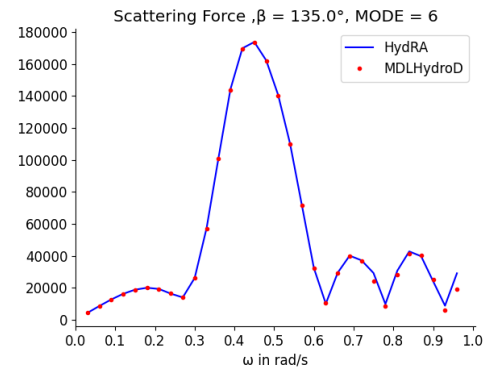
(e) Pitch ScFrc $\beta = 135°$

(f) Yaw ScFrc $\beta = 135°$

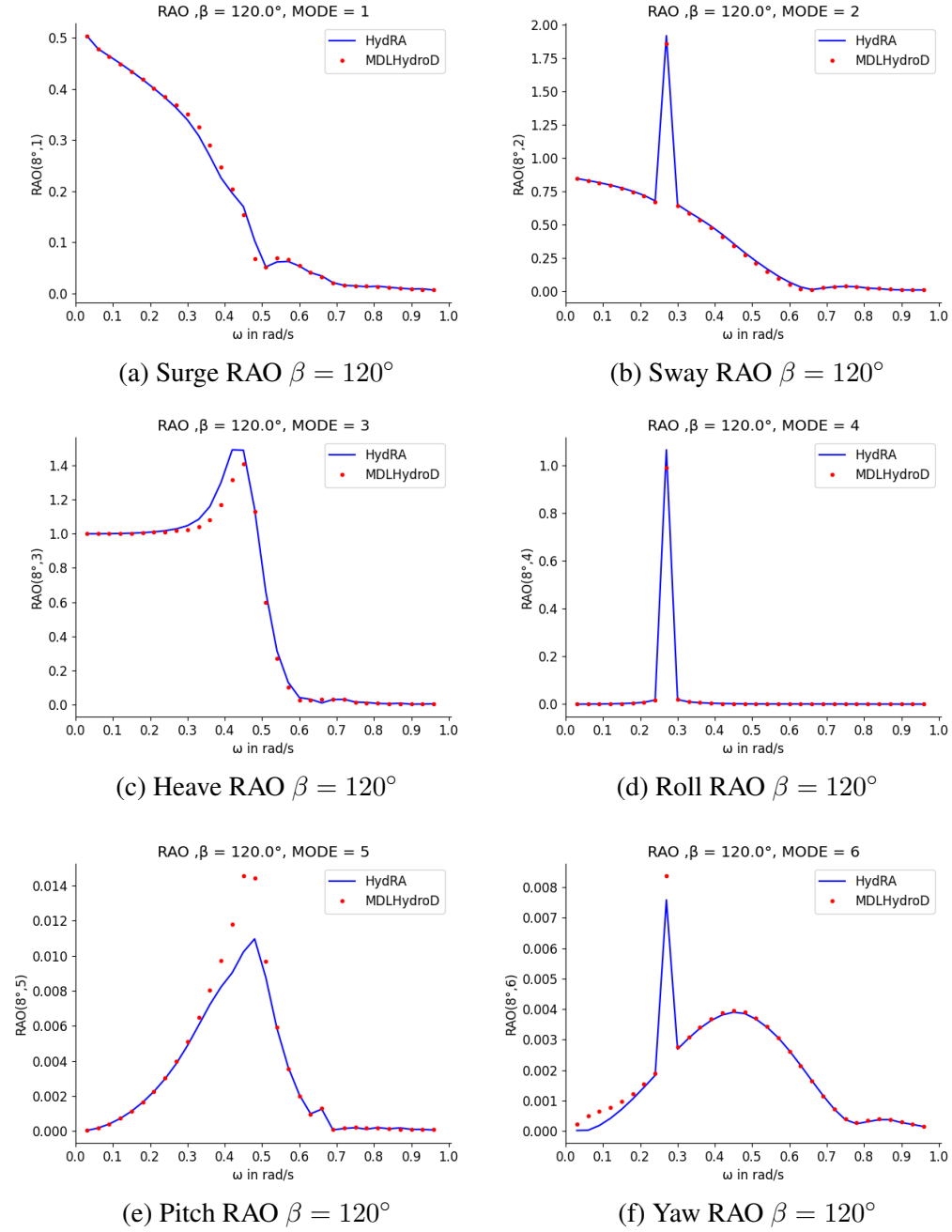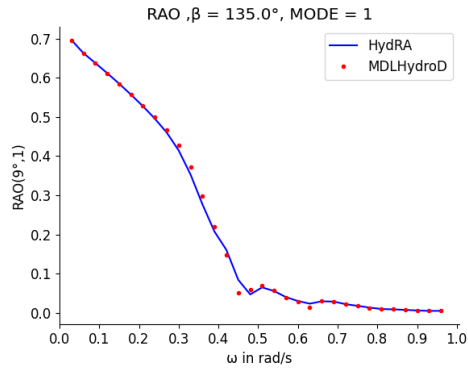Figure 6.10: KVLCC2 vessel Scattering force comparison for $\beta = 135°$

6.2.5   RAO

(a) Surge RAO $\beta = 120°$

(b) Sway RAO $\beta = 120°$

(c) Heave RAO $\beta = 120°$

(d) Roll RAO $\beta = 120°$
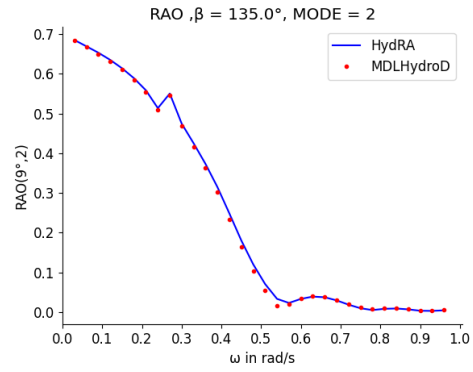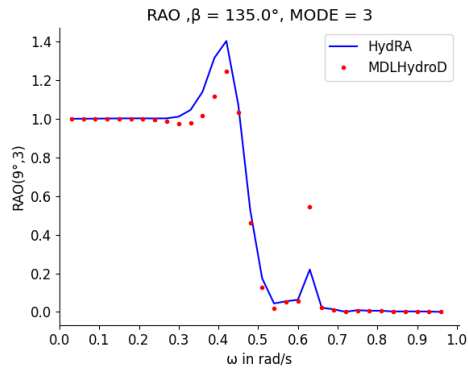
(e) Pitch RAO $\beta = 120°$

(f) Yaw RAO $\beta = 120°$
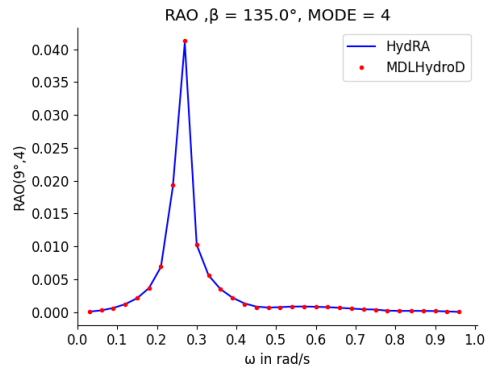
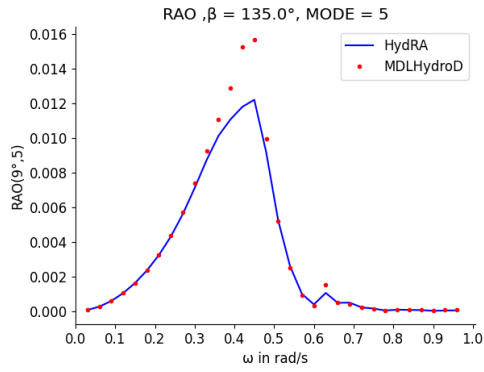Figure 6.11: KVLCC2 vessel RAO comparison for $\beta = 120°$
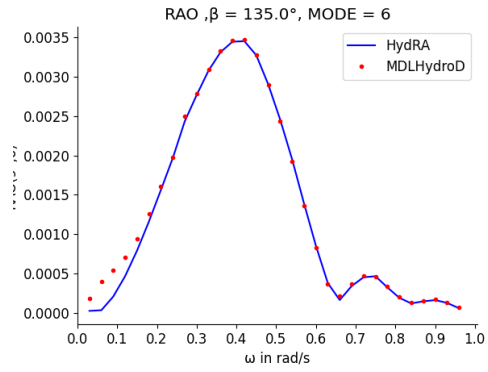
(a) Surge RAO $\beta = 135°$

(b) Sway RAO $\beta = 135°$

(c) Heave RAO $\beta = 135°$

(d) Roll RAO $\beta = 135°$

(e) Pitch RAO $\beta = 135°$

(f) Yaw RAO $\beta = 135°$

Figure 6.12: KVLCC2 vessel RAO comparison for $\beta = 135°$

6.3 Drift force comparisons

Generally, in resistance prediction methods, the influence of the hull emergence angle is often disregarded or ignored. While far-field methods are believed to be unaffected by minor variations in the hull shape, near-field methods factor in the relative wave amplitude across the waterline to calculate the added resistance. Effect of hull emergence is explained in detail in Guha and Falzarano (2015*a*). After, incorporating the effect of hull emergence angle the actual value of Mean drift force is found lessor. This effect is shown in the below comparisons with WAMIT6. WAMIT6 does not consider hull emergence angle. Comparisons are done for KCS vessel, whose principal parameters are give in table (6.1). The input parameters are same as used for forward speed comparisons.
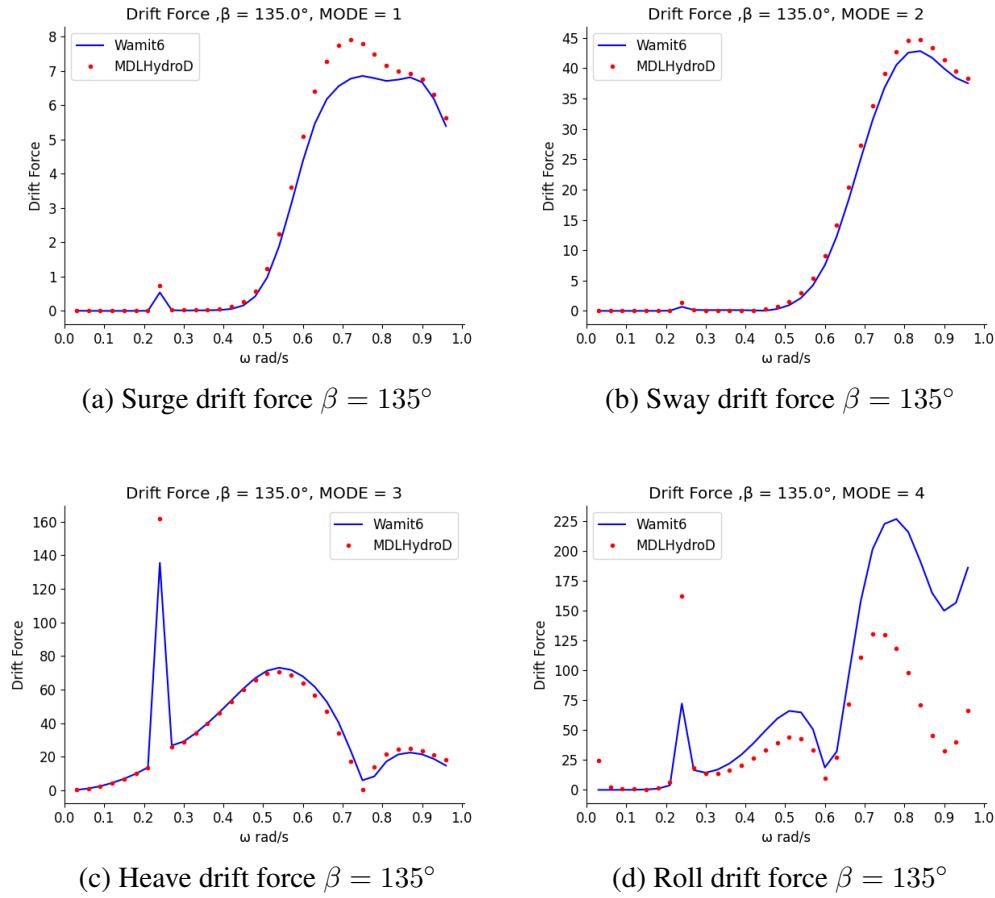

(a) Surge drift force $\beta = 135°$

(b) Sway drift force $\beta = 135°$

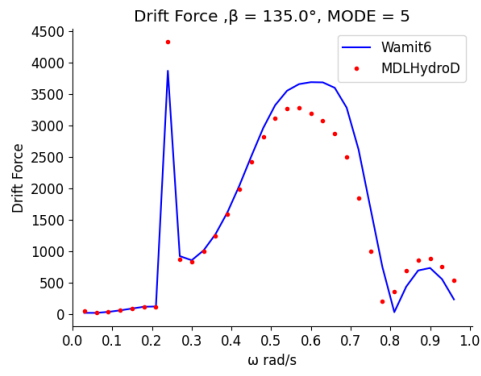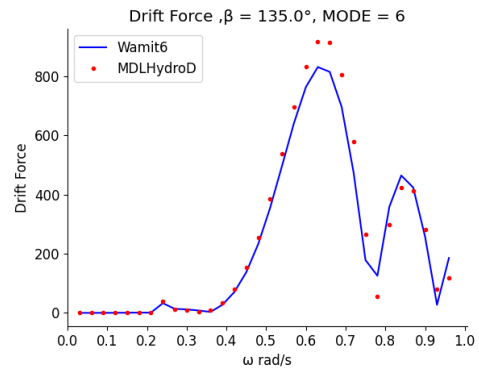(c) Heave drift force $\beta = 135°$

(d) Roll drift force $\beta = 135°$

Figure 6.13: KCS vessel Drift force-I comparison for $\beta = 135°$

(a) Pitch drift force $\beta = 135°$ (b) Yaw drift force $\beta = 135°$

Figure 6.14: KCS vessel Drift force-II comparison for $\beta = 135°$

CHAPTER 7

CONCLUSION

A new numerical tool is developed using a web-based frequency domain approach for calculating hydrodynamic forces and motions at low to moderate forward speeds. To account for the effect of forward speed, incident frequencies were adjusted to encounter frequencies using the Doppler effect. Additionally, boundary conditions are modified by incorporating forward speed U and encounter frequencies. The accuracy of the proposed method was verified by comparing the results against those obtained from the MDLHydroD software for the KCS and KVLCC2 vessel hull structures. While programming, the code is implemented in such a way that the simulation can be performed for both single body case and multiple body case, which is an advantage over MDLHydroD. The computed drift forces are determined using perturbation theory, and the second-order force and moment terms were obtained by considering perturbation parameter terms up to the second degree. A comparison of the drift force between MDLHydroD and WAMIT6 is also performed, where it is found that the value of drift force is lower for some modes of motion in MDLHydroD due to its implementation of hull emergence angle. The results of this study demonstrate good agreement with the MDLHydroD software and provide valuable insights into the hydrodynamic forces and motions of vessels at low to moderate forward speeds. However, due to time constraints code for the drift force part is not implemented in the HydRA program. In the thesis, drift force theory alone is explained.

REFERENCES

1. **Beck, R. F.** and **A. W. Troesch** (1990). Documentation and user's manual for the computer program shipmo. *Department of Naval Architecture and Marine Engineering, The University of Michigan.*

2. **Boese, P.** (1970). Eine einfache methode zur berechnung der widerstandserhöhung eines schiffes im seegang. Technical report.

3. **Faltinsen, O. M.**, Prediction of resistance and propulsion of a ship in a seaway. *In 13th Symposium on Naval Hydrodynamics, Tokyo.* 1980.

4. **Guha, A.** (2012). *Development of a computer program for three dimensional frequency domain analysis of zero speed first order wave body interaction.* Ph.D. thesis.

5. **Guha, A.** and **J. Falzarano**, Development of a computer program for three dimensional analysis of zero speed first order wave body interaction in frequency domain. *In International Conference on Offshore Mechanics and Arctic Engineering*, volume 55393. American Society of Mechanical Engineers, 2013.

6. **Guha, A.** and **J. Falzarano** (2015*a*). The effect of hull emergence angle on the near field formulation of added resistance. *Ocean Engineering*, **105**, 10–24.

7. **Guha, A.** and **J. Falzarano** (2015*b*). Estimation of hydrodynamic forces and motion of ships with steady forward speed. *International Shipbuilding Progress*, **62**(3-4), 113–138.

8. **Hess, J. L.** and **A. M. O. Smith** (1964). Calculation of nonlifting potential flow about arbitrary three-dimensional bodies. *Journal of ship research*, **8**(04), 22–44.

9. **Journée, J.** (2001). Theoretical manual of seaway. *Delft University of Technology Shiphydromechanics Laboratory,(Release 4.19, 12-02-2001), http://www. shipmotions. nl/DUT/PapersReports/1370-StripTheory-03. pdf*.

10. **Katz, J.** and **A. Plotkin**, *Low-speed aerodynamics*, volume 13. Cambridge university press, 2001.

11. **Liapis, S. J.**, *Time-domain analysis of ship motions*. University of Michigan, 1986.

12. **Maruo, H.** (1957). The excess resistance of a ship in rough seas. *International Shipbuilding Progress*, **4**(35), 337–345.

13. **Newman, J. N.** (1979). The theory of ship motions. *Advances in applied mechanics*, **18**, 221–283.

14. **Ogilvie, T. F.** and **E. O. Tuck** (1969). A rational strip theory of ship motions: part i. Technical report, University of Michigan.

15. **Pinkster, J. A.** (1980). Low frequency second order wave exciting forces on floating structures.

16. **Salvesen, N.**, **E. Tuck**, and **O. Faltinsen** (1970). Ship motions and sea loads.

17. **Telste, J.** and **F. Noblesse** (1986). Numerical evaluation of the green function of water-wave radiation and diffraction. *Journal of Ship Research*, **30**(02), 69–84.